RESEARCH ARTICLE

Nature Inspired Approach Toward Elimination of Nonlinearities in SWIPT Enabled Energy Harvesting Networks

AJIN R. NAIR, (Graduate Student Member, IEEE), AND S. KIRTHIGA
Department of Electronics and Communication Engineering, Amrita School of Engineering Coimbatore, Amrita Vishwa Vidyapeetham, Coimbatore 641112, India

Corresponding author: S. Kirthiga (s_krithiga@cb.amrita.edu)

ABSTRACT The greatest challenge faced by the Simultaneous Wireless Information and Power Transfer (SWIPT) system during implementation is hardware impairment. This article proposes a bio-inspired digital pre-distortion scheme to overcome the high power amplifier nonlinearity and in-phase and quadrature imbalances in the SWIPT system. Here, the memory polynomial model characterises the high power amplifier. The digital pre-distortion algorithm uses the latest bio-inspired methods: Dingo Optimization, Jumping Spider Optimization, Seagull Optimization, Mexican Axolotl Optimization, and Black Widow Optimization. The power conversion efficiency, harvested energy, and rate energy region at the receiver side analyse the efficiency of bio-inspired digital pre-distortion enabled SWIPT. Among the various bio-inspired algorithms, the Seagull Optimisation Algorithm gave a maximum harvested energy of 35.95 μW, keeping a Bit Error Rate of 1.33×10^{-6} for the 32-QAM scheme. The Seagull Optimisation Algorithm also showed a maximum improvement of 6.45% in power conversion efficiency compared to the conventional digital pre-distortion scheme.

INDEX TERMS Bio-inspired, digital pre-distortion (DPD), energy harvesting, high power amplifier (HPA) nonlinearity, hardware impairments, in-phase and quadrature (IQ) imbalance, simultaneous wireless information and power transfer (SWIPT).

I. INTRODUCTION

The Simultaneous Wireless Information and Power Transfer (SWIPT) enabled Energy Harvesting (EH) is a trending technology and a possible candidate for 6G enabled wireless communication networks [1]. The SWIPT technology, which performs information transfer and power extraction simultaneously, was initially proposed in "Transporting information and energy simultaneously" by Varshney [2]. It is inspired by green communications that create self-sustainable wireless nodes. The SWIPT technology can provide power to far away nodes that face severe fading conditions

The practical implementation of SWIPT is performed mainly through two architectures: Time Switching (TS) and Power Splitting (PS). The separation of information and energy is performed in the time domain for TS architecture.

The associate editor coordinating the review of this manuscript and approving it for publication was Agustin Leobardo Herrera-May.

Conversely, the separation is accomplished through the power domain in PS architecture. In Kang *et al.* [3], the ideal information transmission model based on SWIPT PS and TS architectures is discussed. However, as given in Perera *et al.* [4], the practical implementation of SWIPT brings in many challenges in the form of hardware impairments such as IQ (In-phase and Quadrature-phase) imbalance and High Power Amplifier (HPA) nonlinearities.

The IQ imbalance that is caused due to the non-orthogonality of I and Q branches at transmitter and receiver sections is elaborated in Schenk [5]. This non-orthogonality is expressed in terms of amplitude imbalance and phase imbalance. The IQ imbalance distorts signal constellation during decoding operation and affects symbol detection rate. For 0.2 dB imbalance in amplitude and 2^0 of imbalance in phase at transmitter produces 25dB of carrier suppression. This imbalance will reduce the signal-to-noise ratio (SNR) by 1dB at the receiver side, as mentioned in Tsou [6].

In Nair *et al.* [7], the estimation and compensation with SNR and BER (Bit Error Rate) performance analysis for the SWIPT PS system under IQ imbalance is investigated. Also, a bio-inspired approach to analyze energy harvesting in SWIPT system under IQ imbalance was performed in Nair *et al.* [8]. For the last few years, despite the mentions in the literature about IQ imbalance problems that affect SWIPT performance, a few have tried to address them.

The SWIPT must use high-power transmitters to harvest significant energy during implementation. So the impairments due to HPA nonlinearities gain more importance in SWIPT systems when compared to typical wireless communication systems. Also, the efficiency of the SWIPT system is dependent on HPA performance. The initial efforts to study the effect of HPA nonlinearities and HPA harmonics in the SWIPT system were made in Jang *et al.* [9] and Nair and Kirthiga [10] respectively. Here the power spectrum showed a decrease of 23 dBc in the presence of HPA nonlinearity and approximately 3dB reduction in output power. There are multi-tone methods suggested in Park *et al.* [11] for compensation of HPA nonlinearities in the SWIPT system. Also, the SWIPT system adopting practical M-ary modulation without considering any nonlinearities was first mentioned in Liu *et al.* [12]. But, to the best of our knowledge, no work in the literature has analyzed the combined effect of HPA nonlinearity and IQ imbalances in SWIPT-enabled wireless communication systems under M-ary modulation schemes. However, performing critical impact analysis and suggesting compensation for nonlinearities in SWIPT under existing M-ary modulation schemes is essential.

Two conventional remedies are suggested to overcome HPA nonlinearities in Radio Frequency (RF) systems, as indicated by Schenk [5]. The first is to use linear components in the RF front end, and the second is to put in measures for input power backoff before feeding the signals to RF amplifiers. The drawback of the first remedy is that it increases the total cost incurred in the RF front end. The second remedy is inefficient in terms of power consumption and efficiency. The input backoff in the -5dB to 15dB range for SWIPT delivers only an average PA efficiency of about 60% as mentioned in Chen *et al.* [13]. However, integrating Digital Pre-Distortion (DPD) into the communication setup allows the transmitter to operate near or above the saturation point of the PA, thereby eliminating the need for input power backoff. Even though the DPD solution's cost is more, it can be quickly recovered in two years due to its reduced electricity consumption. Moreover, the DPD can combine more than one nonlinearity problem in the RF front end, as mentioned in Sun *et al.* [14]. Therefore, a Digital Pre-distortion Algorithm (DPA) is suggested to circumvent the IQ imbalance and HPA nonlinearity problem in SWIPT. The DPA measures the presence of nonlinearities in HPA and computes an inverse operation to linearise the HPA effectively. Joint mitigation of IQ imbalance and HPA nonlinearity in MIMO systems using DPA is discussed in Khan *et al.* [15]. In Mukherjee *et al.* [16], an adaptive

algorithm for estimating HPA nonlinearity in the SWIPT system is first proposed. Also, bio-inspired algorithms like Particle Swarm Optimization (PSO), Grey Wolf Optimizer (GWO), Hybrid PSO-GWO algorithm (HPSOGWO), and Binary Coyote Optimization Algorithm (BCOA) are suitable for solving complex engineering problems, as mentioned in Negi *et al.* [17] and Leandro *et al.* [18], [19]. The DPA based on bio-inspired algorithms applied to typical wireless communication systems is also efficient. A PSO algorithm-based digital pre-distorter is used in Abdelhafiz *et al.* [20]. The HPA linearization using Artificial Bee Colony (ABC) was performed in Bipin and Rao [21]. The DPA based on Hill-Climbing (HC) heuristics and Genetic Algorithm (GA) is performed in Wang [22].

There are several models available for representing the nonlinearities in HPA. These models capture Amplitude-to-Amplitude (AM-AM) distortion or Amplitude dependent Phase (AM-PM) distortion or both, as mentioned in Tsou *et al.* [23]. The AM-AM distortion represents nonlinearity as the difference in input voltage and the envelope of RF amplifier output. The AM-PM distortion is the undesired phase modulation generated in the RF amplifier output due to the nonlinear capacitors and power supply variations in input voltage. The commonly used models for HPA are ideal clipping amplifier, travelling wave tube amplifier, solid-state amplifier, and memory polynomial models. The ideal clipping amplifier, which captures only the AM-AM distortion, shows the clipping of amplifier input beyond the PA saturation level. The travelling wave tube amplifier, which can work in broad ranges, can capture both AM-AM and AM-PM distortion but has a disadvantage of very low power efficiency as described in Paoloni *et al.* [24]. The solid-state power amplifier (SSPA) that resembles the behaviour of HPA can capture only AM-AM distortion, as mentioned in Khalfet and Krikidis [25]. The HPA is best modelled by the memory polynomial model that simultaneously captures AM-AM and AM-PM distortion, as described in Kim and Konstantinou [26].

In Huang *et al.* [27], the general energy harvesting models used in wireless communication are mentioned. These energy harvesting models are used in [28], [29], and [30] for solving energy maximization problems in wireless networks. In Liu *et al.* [12], a practical visualization of energy harvesting with an M-ary modulation scheme in the SWIPT system was implemented. Nevertheless, these energy harvesting models mentioned above do not incorporate the hardware impairment aspects. The following observations from the literature helped to frame the proposed problem. 1) There are only a few works in literature that focus on the practical implementation of SWIPT involving hardware impairments such as IQ imbalance and HPA nonlinearities. [4]. 2) DPD can combine more than one problem Sun *et al.* [14]. 3) A conventional DPD, when applied to the SWIPT system with HPA nonlinearities, yielded good results. [16]. 4) A bio-inspired DPD performs well in typical wireless communication systems [20], [21], [22].

Since the SWIPT system needs to derive a significant amount of energy, Power Conversion Efficiency (PCE) appearing because of RF to DC conversion should also be considered a hardware impairment in the SWIPT system. The overall efficiency of the SWIPT system has to be visualized through the Rate Energy (RE) region.

In this article DPD assisted SWIPT is simulated and analyzed using the latest and efficient bio-inspired techniques such as Dingo Optimization algorithm (DOA) [31], Jumping Spider Optimization algorithm (JSOA) [32], Seagull Optimization algorithm (SOA) [33], Mexican Axolotl Optimization (MAO) [34] and Black Widow Optimization algorithm (BWOA) [35]. The scientific contribution ingrained in this article is the bio-inspired DPD applied to the SWIPT system having both IQ imbalance, and HPA nonlinearity impairment. The efficiency of bio-inspired DPD assisted SWIPT is analyzed through PCE and RE for the basic M-ary modulation schemes.

The article is organized as follows. Section II describes the system used for the HPA model and DPA in SWIPT. The nature inspired approach towards nonlinearities in SWIPT is explained in Section III. Section IV shows the simulation results and discussions regarding the specific model discussed in the previous section. The article's conclusions are given in Section V.

II. SYSTEM DESCRIPTION

The SWIPT system and its intended implementation style are shown in Figure 1. The diagram indicates that the SWIPT wireless system enables simultaneous power and information transfer. Since it is a concurrent transmission process, there is always a compromise between the harvested energy and information rate. There are four possible architectures mentioned in Perera *et al.* [4] for the SWIPT system: power splitting, antenna switching, time switching, and separate receiver architecture. Here, the PS architecture poses the advantage in time resource and information rate compared to TS [8].

A. TRANSMITTER SECTION

The essential blocks involved in DPD enabled SWIPT transmitter is shown in Figure 2. The various components of the SWIPT transmitter can be realized using IQ modulators and demodulators, data converters, filters, mixers, HPAs', attenuators etc. The Digital Signal Processing (DSP) domain involves baseband signal processing to generate the I (Real) and Q (Imaginary) parts of the input signal. The digital modulation considered at the baseband is M-ary Quadrature Amplitude Modulation (M-QAM), given by

$$M = 2^k \tag{1}$$

where M represents the unique number of bits transmitted per time interval and k is an integer. As given in Najatizadeh and Tellambura [36], the complex envelope of message signal is represented with real and imaginary parts as

$$x = x_I + j\,x_Q \tag{2}$$

where the in-phase component and the quadrature component of x is represented by x_I and x_Q respectively. The x_I and x_Q components are given by

$$x_I \in \{\pm a, \pm 3a, \ldots (I - 1)a\} \tag{3}$$

$$x_Q \in \{\pm a, \pm 3a, \ldots (J - 1)a\} \tag{4}$$

where $I = 2^{(m-1)/2}$, $J = 2^{(m+1)/2}$ and $2a$ is the distance between adjacent points in the QAM constellation. As the 'M' value increases for the QAM scheme, the bit energy E_b also increases, which is given by

$$E_b = \frac{M - 1}{3log_2(M)} E_g \tag{5}$$

where E_g represents energy of the input signal pulse

The DSP domain also performs predistortion to the desired signal. After the data conversion from digital to analog, the signals are filtered via a low pass filter. Then mixer will multiply the I and Q signals with the help of the local oscillator (LO). Here the I and Q signals are orthogonal to each other. Any mismatch in orthogonality of I and Q is accounted as IQ imbalance. The transmitter section considers an imbalance of 0.2 dB in amplitude and 2° in phase. After bandpass filtering, the combined I and Q signals are amplified using HPA and transmitted using an antenna module. The practical HPA exhibits nonlinearities during amplification; therefore, we need nonlinear models. The DPD-enabled SWIPT transmitter is also integrated with a feedback observation path to correct the input signal. The observation path will detect the PA's nonlinearity or distortion. The DPD system will compare the power amplifier output with the input baseband signal and apply distortion to the power amplifier input until the HPA output replicates the input baseband signal. The distortion function variables are continuously changed to reduce the difference in the baseband signal and the HPA output. In practice, HPA exhibits memory effects where the current output depends on the previous input samples. Modelling HPA accounting memory effects is a significant challenge in transmitter systems. The modelling becomes more relevant for SWIPT systems that harvest more power using HPAs'. The nonlinearity of the HPA can be effectively captured with the help of the memory polynomial model, which is discussed in the next section.

1) MEMORY POLYNOMIAL MODEL FOR HPA

The model of the HPA is obtained from AM-AM and AM-PM characteristics by the curve fitting method. The most commonly used model for curve fitting is the polynomial fitting model. The polynomial fitting model is obtained through the least-squares procedure, which minimizes the Euclidean distance between the curve fitting function and the input data. But the least-squares approach is based on instantaneous values and will not capture any memory effect. To include the memory effect, we must find a model that explicitly retains the record of the time domain in its formulation. In this case, using a Volterra series polynomial will be the best method to include the memory effects. The precision of the Volterra
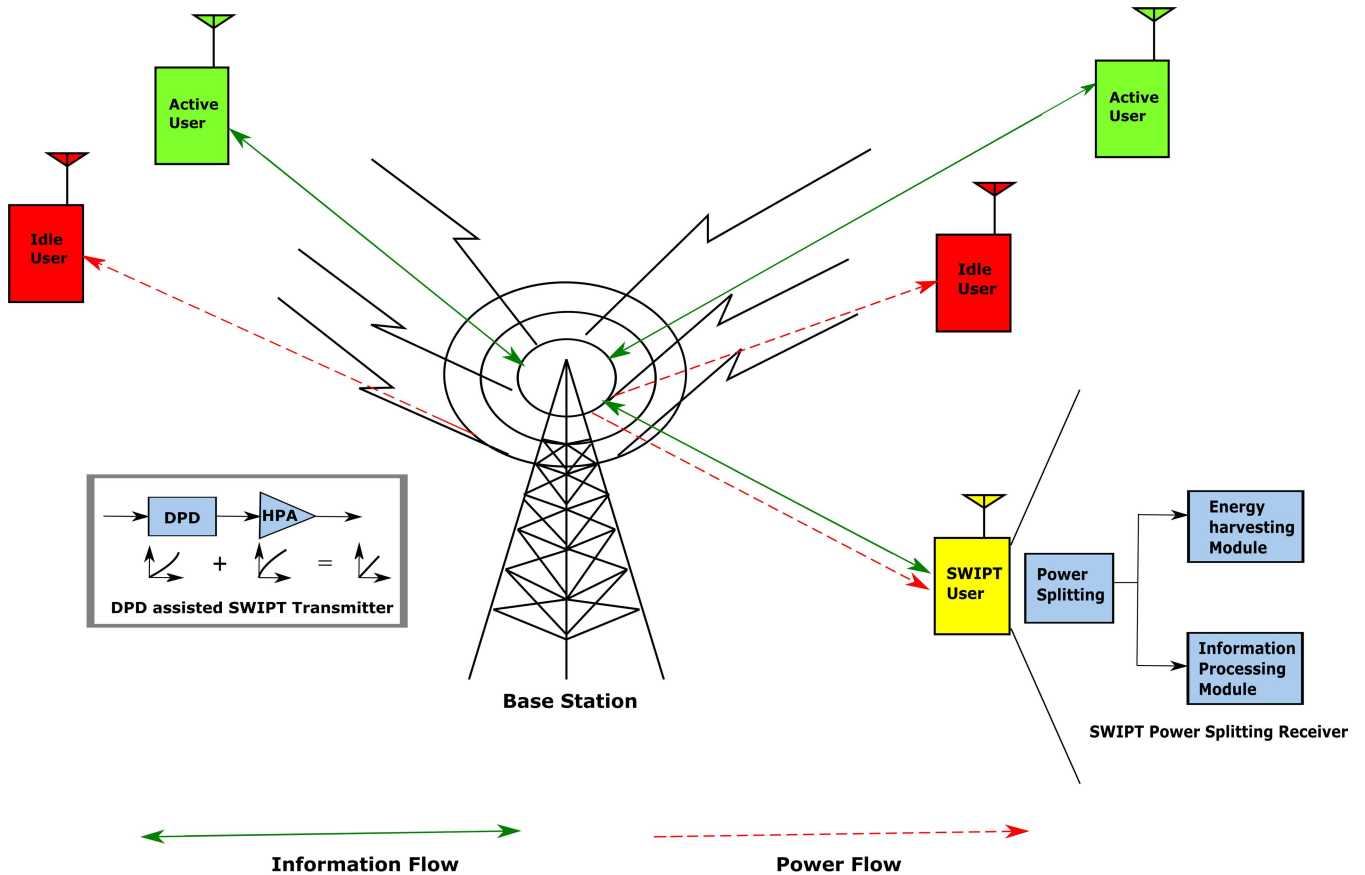
FIGURE 1. Three types of users are generally considered under the SWIPT scenario. Here, the direction of information and power flow is indicated with the help of arrowheads. The user involved in information transfer alone is regarded as an active user. The users who are not engaged in information transfer will harvest energy from the base station. On the other hand, a SWIPT user adopting a power splitting scheme indulges in information and power transfer simultaneously. In all the user cases, the transmitter uses DPD to compensate for IQ imbalance and amplifier non-linearities. Note: The co-existing multiuser cases are not considered in this representation, but discuss the possibility of different users under the SWIPT scenario.
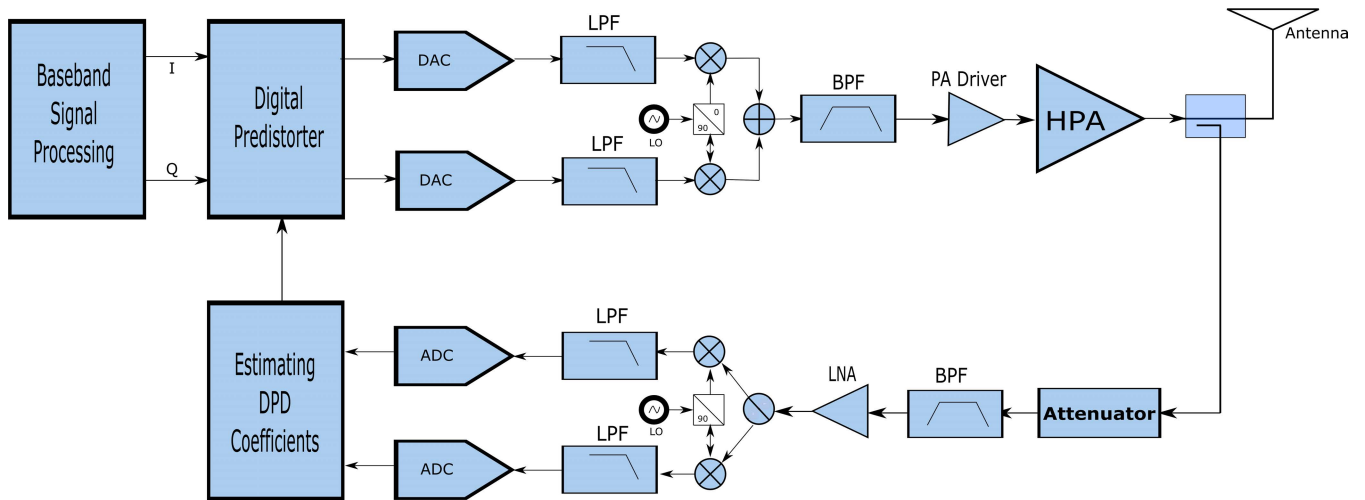

FIGURE 2. Transmitter model.

model rises with the number of terms in polynomial series, polynomial degree and memory depth. Further, the inclusion of cross-terms increases the number of terms and improves the accuracy of the Volterra model.

As mentioned before, HPA nonlinearity will degrade the system performance. The output of practical HPA will depend on the present and previous HPA input signals. This dynamic behaviour of HPA is captured with the polynomial model.
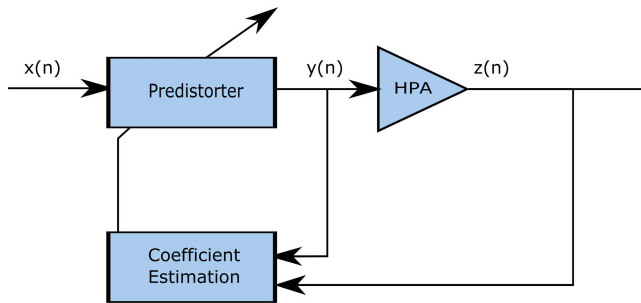
FIGURE 3. General Predistortion scheme.

Figure 3 depicts the general approach toward nonlinearity with memory based on the Volterra series. The baseband $x(n)$ is fed to the DPD unit to yield the predistorted output $y(n)$. This predistorted output is given to the HPA to generate linear output $z(n)$. The Volterra series is nothing but a multidimensional convolution sum. The T-tap finite memory representation of Volterra series with d dimensions and k_d kernel as mentioned in Schetzen [37] is given by (6).

$$z(n) = \sum_{d=1}^{D} z_d(n) \qquad (6)$$

where

$$z_d(n) = \sum_{t_1=0}^{T-1} \cdots \sum_{t_d=0}^{T-1} k_d(t_1, \ldots, t_d) \prod_{i=1}^{d} y(n - t_i),$$
$$i = 1, 2, \ldots, d-1 \qquad (7)$$

Here, changing the index variables makes it possible to bring out the significant diagonal entries as indicated in Raz and Van Veen [38].

$$n_i = t_{i+1} - t_i \qquad (8)$$

$$z_d(n) = \sum_{n_1=-T+1}^{T-1} \sum_{n_2=-T+1}^{T-1} \cdots \sum_{n_{d-1}=-T+1}^{T-1} h^d_{n_1,\ldots,n_{d-1}}(n)$$
$$* \left[y(n) \prod_{i=1}^{d-1} y(n - n_i) \right] \qquad (9)$$

Here $*$ represents one-dimensional convolution with

$$h^d_{n_1,\ldots,n_{d-1}}(n) = k_d(n, n + n_1, \ldots, n + n_{d-1}) \qquad (10)$$

From (10), it is clear that d^{th} order Volterra output is nothing but the sum of linear filter outputs. Also, the filter input would be the multiplication of d different time shifts of the input signal given by

$$y(n) \prod_{i=1}^{d-1} y(n - n_i) \qquad (11)$$

The memory polynomial model is nothing but a particular case of the Hammerstein model. [39]. The Hammerstein

model is given by

$$z_H(n) = \sum_{d=1}^{D} \sum_{t=0}^{T-1} p_{dt} \, y^d(n - t) \quad d = 1, 2, \ldots, D \qquad (12)$$

where p_{dt} is a two-dimensional array representing the polynomial non-linearity coefficients. Here, high sampling rate is considered such that all the products up to D order are alias-free. Choosing $y(n)|y(n - t)|^{d-1}$ combinations [26] from the Hammerstein model, we arrive at the polynomial model.

$$z_P(n) = \sum_{d=0}^{D-1} \sum_{t=0}^{T-1} p_{dt} \, y(n - t)|y(n - t)|^d \qquad (13)$$

Here index d represents the order of envelope. If we observe in (13), the input samples $y^d(n - t)$ are considered at the same time instant. Now, through Wiener model [40] we can easily include cross terms that represents memory effects. The Wiener model is given by

$$z_W(n) = \sum_{d=1}^{D} p_d \left[\sum_{t=0}^{T-1} k(t) y(n - t) \right]^d \qquad (14)$$

Using (9) and (11), we can find out cross-terms that represents memory effects. Also, by looking into (13) and (14), we can gather these cross terms and represent them as

$$\sum_{d=0}^{D-1} q_d \, y(n) \left[\sum_{t=0}^{T-1} r_t |y(n - t)| \right]^d \qquad (15)$$

where q_d and r_t represent the polynomial nonlinearity coefficients and envelope filter coefficients, respectively. Combining (13) and (15), the memory polynomial is obtained as

$$z_{MP}(n) = \sum_{d=0}^{D-1} \sum_{t=0}^{T-1} p_{dt} y(n - t)|y(n - t)|^d$$
$$+ \sum_{d=1}^{D-1} q_d y(n) \left[\sum_{t=0}^{T-1} r_t |y(n - t)| \right]^d \qquad (16)$$

The p_{dt} and q_d coefficients are estimated using least-squares solution, keeping r_t fixed. The memory polynomial model with cross terms is a better representation that mimics amplifier nonlinearity when compared with the polynomial model.

2) DPD COEFFICIENT ESTIMATION
As discussed before, DPD can combine more than one type of nonlinearity. So, we consider the blended influence of HPA nonlinearity and IQ imbalance in the transmitter system. The HPA nonlinearities will include compression and memory effects. As discussed previously, the Volterra model will capture HPA nonlinearity. The DPD compare the input signal and HPA output to estimate error. The DPD algorithm will be adapted to minimize the error in the subsequent calculation. The least mean squares (LMS) method calculates the new set of DPD coefficients. Finding the new set of DPD coefficients is by deriving the pth order inverse from the memory amplifier output [37]. Since the inverse model is obtained as the output
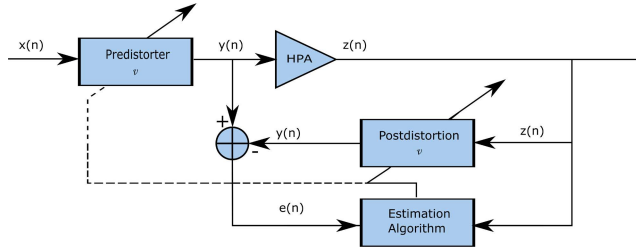
FIGURE 4. Inverse model for Predistortion.

FIGURE 5. IQ imbalance model.

of the amplifier, we call it post-distortion. The model is shown in Figure 4.

To perform estimation, first, all the C coefficients are collected to form a vector v with dimension $C \times 1$. Each component of v is associated with the signal having time samples over the period t $= 1, 2, \ldots,$ T. The time samples form a vector with $T \times 1$ dimension. Gathering these vectors together, we create the matrix Y with dimension $T \times C$ expressed as

$$\hat{z} = Yv \tag{17}$$

Similarly, the inverse operation can be written as

$$\hat{y} = Zv \tag{18}$$

The estimation error from the Figure 4 is expressed as

$$e(n) = y(n) - \hat{y}(n) \tag{19}$$

The vector form of error is represented as

$$e = y - \hat{y} \tag{20}$$

The least square solution that minimizes $\|e\|^2$ is given by

$$v = (Z^H Z)^{-1} Z^H y \tag{21}$$

The solution of (21) can be obtained using the Cholesky decomposition method by representing the set of linear equations in the form.

$$Z^H Zv = Z^H y \tag{22}$$

3) IQ MODULATION AND DEMODULATION
As mentioned, the feedback observation path critically impacts the transmitter's overall performance and capability. In our analysis of the feedback observation path, we consider the IQ demodulator impairment. The impairments contain noise injection from the local oscillator (LO) due to phase noise and the interference in the I and Q paths of the demodulator. The impairments during IQ demodulation are visualized through the model [41] given in Figure 5. The imbalance in amplitude is modelled with the help of two linear gain amplifiers, U and V. The imbalance in phase ω observed between I and Q paths are represented by cross-talk among the two amplifiers.
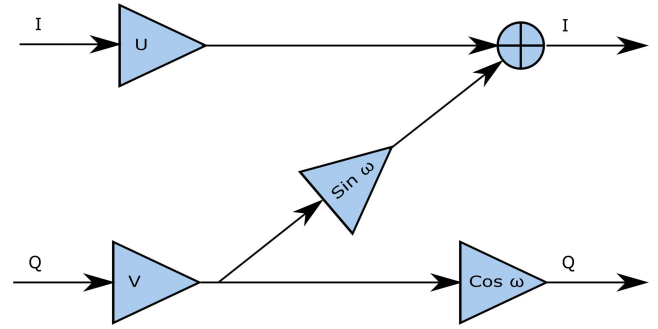
The modulated QAM signal is applied with a square-root raised cosine (RRC) filter to perform pulse shaping and eliminate intersymbol interference (ISI). The window function used in the RRC filtering operation is given by [42]

$$RRC = \frac{cos(\frac{\pi \alpha t}{T})}{1 - (\frac{2\alpha t}{T})^2} \tag{23}$$

Here α is the roll-of factor, and T represents filter length. Similarly, another RRC filter has to be included before demodulation to remove ISI.

4) AMPLIFIERS AND FILTERS
The PA driver amplifiers are considered ideal and do not contribute much to the nonlinearity. Any distortion generated by the PA driver will arise in the HPA response, and the DPD can accommodate them. Since the significant contributor to nonlinearity is HPA, it is essential to describe the HPA model correctly. In the feedback path, the level of noise or sensitivity of the DPD is with the low-noise amplifier (LNA) as discussed in Campo *et al.* [43]. Thus the LNA plays a significant role in the observation path. Also, the passive components like filters and attenuators influence the frequency characteristics and the system's input signal levels to the PA drivers and the LNA.

B. RECEIVER SECTION
1) POWER SPLITTING
It is considered that AWGN appears in the channel while receiving the signal at the SWIPT receiver, as shown in Figure 6. The SWIPT receiver employs a power splitting scheme at the receiver side. The PS architecture unfolds the practical model that involves a concurrent transmission of information and power. In the PS method, the signal is split in the power domain with $\rho \in (0, 1)$ as the PS factor. The PS factor determines the amount of power given to the energy harvesting module. The remaining $1 - \rho$ power is provided to the Information Processing (IP) module.

2) ENERGY HARVESTING MODULE
Overall, RF-to-DC conversion and energy storage occur in the energy harvesting module. The role of the antenna in an energy harvesting circuit is to capture RF signals. The
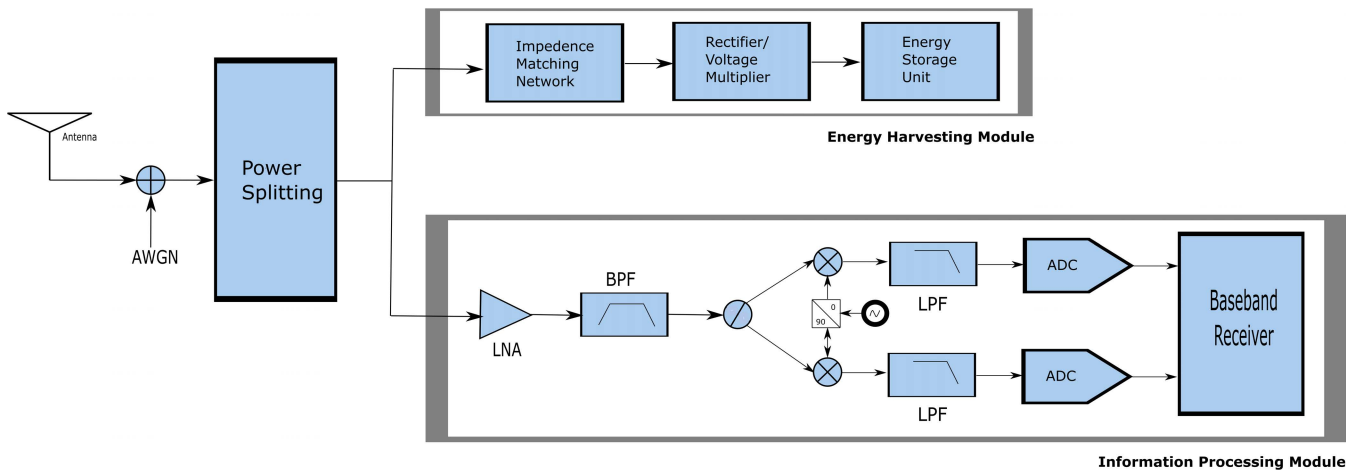
FIGURE 6. Receiver model.

antenna's gain, frequency, and efficiency hold a significant role in the successful operation of the energy harvesting circuit, as conveyed in Cansiz *et al.* [44]. As mentioned in Perez [45], the impedance matching reduces signal reflections and guarantees maximum power transfer between the input antenna output and the Rectifier/Voltage Multiplier (RVM). Also, transmission loss from the antenna to the RVM circuit is reduced through impedance matching. So, if we use multiple antennas for energy harvesting modules, the proper impedance matching yields maximum harvested energy. Another issue in RVM is that the nonlinear components reduce the PCE of the energy harvesting circuit. The diode's nonlinear characteristics and saturation effects at high received power significantly contribute to RVM nonlinearity, as mentioned in Bonnin *et al.* [46]. Also, suppose the distance from the transmitter to the energy harvesting module increases. In that case, the transmitter's drive power must also increase to maintain the minimum turn-on power required for the diode to operate. The harvested energy from the RVM module is stored in an energy storage unit. The storage unit can be a battery or a supercapacitor. Overall, energy harvesting is performed when there is a need to extend the user node's lifetime. The harvested energy in the energy harvesting module is given by [8]

$$Y_{eh} = \eta \rho P_T |h|^2 T \qquad (24)$$

η represents PCE, P_T indicates transmitted power, h is the channel's gain, and T is the duration of the transmission. PCE is given by [16]

$$\eta = \frac{Y_{eh}}{P_R} \qquad (25)$$

P_R represents the received power.

3) INFORMATION PROCESSING MODULE

The LNA boosts the received signal well above the noise floor in the information processing module. Along with LNA,

the BPF isolates the receiver to decode only the signal frequencies of interest. The signal output from BPF is split and applied to the mixer. The mixer generates the in-phase signal output with the help of a local oscillator (LO). Similarly, the quadrature is obtained using the 90° phase-shifted quadrature oscillator signal. To remove any spectral tributaries, we apply LPF after demodulation. After analog to digital conversion, the I and Q parts of the signal is successfully decoded at the baseband receiver. The SNR of the information processing module is measured in the presence of amplitude imbalance α and phase imbalance ω. This can be expressed as given in [10].

$$SNR_{ip} = \left| \frac{\sqrt{1 - \rho}}{\zeta} \right| \qquad (26)$$

where ζ represents IQ imbalance and is defined as $\zeta = \frac{-\chi}{\psi}$ Here $\chi = cos\omega - j\alpha sin\omega$ and $\psi = \alpha cos\omega + j sin\omega$

The signal obtained at the IP module is expressed as

$$Y_{ip} = \sqrt{SNR_{ip}} \, h \, Z + n \qquad (27)$$

The channel's Additive White Gaussian Noise (AWGN) is denoted by n. The probability of error P_{ip} in the information processing module is given by

$$P_{ip} = \frac{1}{2} \left(1 - erfc \left(\sqrt{\frac{E_b}{N_o}} \right) \right) \qquad (28)$$

where $E_b/N_o(dB) = SNR_{ip}(dB) - 10 \, log(log_2(M))$ is the normalized SNR. Since power splitting is adopted at the receiver side, the harvested energy and information processing rate is done concurrently. The trade-off occurring here can be visualized by the RE analysis, which is given by [8]

$$RE(Y_{eh}, R_{ip}) = \left\{ Y_{eh} \le \eta \rho P_T |h|^2 T, \right.$$

$$\left. R_{ip} \le log_2 \left[1 + SNR_{ip} \right] \right\} \qquad (29)$$

Algorithm 1 Dingo Optimization

1: **procedure** DOA
2: Define the objective function
3: Initialize the parameters of DOA:
     Sea_Age, *Max_Iter*, *Rand_val*, *P_hunt*,
     Q_attack, β_1, β_2, *na_Ini* and *na_End*
4: Initialize Dingo positions
5: **while** *Iter* < *Max_Iter*, **do**
6:   **if** *Rand_val* < *P_hunt*, **then**
7:     **if** *Rand_val* < *Q_attack*, **then**
8:       Perform the group attacking procedure
9:     **else** Perform the persecution procedure
10:     **end if**
11:   **else** Perform the scavenging procedure
12:   **end if**
13:   Update *Sea_Age* having low survival rates
14:   Calculate P_{new}, fitness values of new agents
15:   **if** $P_{new} < P^*$, **then**
16:     $P^* = P_{new}$
17:   **end if**
18:   $Iter = Iter + 1$
19: **end while**
20: Show the optimal solution
21: **end procedure**

---

4) PROBLEM FORMULATION

The formulated problem is to maximize the harvested energy by fine-tuning the PS factor for a SWIPT system subject to RE tradeoff, probability of error and minimizing the mean squared error of DPD.

$$\max_{0 \le \rho \le 1} Y_{eh}$$
$$\text{s.t. C1}: \quad \|\hat{z} - Yv\|^2 \le \|e\|^2$$
$$\text{C2}: \quad R_{ip} \le log_2\left[1 + SNR_{ip}\right]$$
$$\text{C3}: \quad BER \le P_{ip} \quad (30)$$

III. NATURE INSPIRED APPROACH TOWARDS HPA LINEARIZATION

A. DOA APPROACH TOWARDS HPA LINEARIZATION

The DOA that imitates the hunting and social behaviour of Australian dingo dogs is given in Algorithm 1. The algorithm rules are based on three search strategies: attack, group tactics, and scavenging behaviour.

1) GROUP ATTACK PROCEDURE

The dingoes generally form a group and attack prey by finding the location and surrounding it. This attacking procedure is represented by (31).

$$P_i(t+1) = \beta_1 \sum_{k=1}^{na} \frac{\left[A_k(t) - P_i(t)\right]}{na} - P_{best}(t) \quad (31)$$

Here $P_i(t)$ represents current Dingo position, $P_i(t+1)$ represents new Dingo position, $na \in [2, \frac{Sea\_Age}{2}]$, where *Sea_Age* represents number of search agents or Dingoes, $A_k(t)$ subset of total Dingoes that performs attack, where $A \subset P$, P_{best} represent position of the best search agent, $\beta_1 \in [-2, 2]$,

2) PERSECUTION PROCEDURE

Dingos chase the prey and catch them individually. This behaviour can be expressed by (32)

$$P_i(t+1) = P^*(t) + \beta_1 * e^{\beta_2} * (P_n(t) - P_i(t)) \quad (32)$$

Here $\beta_2 \in [-1, 1]$, n is a randomly generated number between 1 and total number of Dingoes, $P_n(t)$ is the nth Dingo selected where $i \ne n$.

3) SCAVENGING PROCEDURE

Dingoes sometimes feed on the decayed flesh of dead animals while roaming around in their habitat. This behaviour can be represented by (33)

$$P_i(t+1) = \frac{1}{2}\left[e^{\beta_2} * P_n(t) - (-1)^{\sigma} * P_i(t)\right] \quad (33)$$

where σ is a randomly generated number, $\sigma \in 0, 1$

4) SURVIVAL RATE

The Dingoes face illegal hunting and are facing the risk of extinction. The survival rate of Dingo is given by

$$Survival(i) = \frac{fitness_{max} - fitness_i}{fitness_{max} - fitness_{min}} \quad (34)$$

Based on (34), Dingo with low survival rates are updated, which is given by

$$P_i(t) = P^*(t) + \frac{1}{2}\left[P_{n1}(t) - (-1)^{\sigma} * P_{n2}(t)\right] \quad (35)$$

where $P_i(t)$ represents Dingo with low survival rate, $n1$ and $n2$ are randomly generated between 1 and total number of Dingoes with $ni \ne n2$, $P_{n1}(t)$ and $P_{n2}(t)$ are the selected search agents.

B. JSOA APPROACH TOWARDS HPA LINEARIZATION

The JSOA is based on the hunting habits of Arachnida Salticidae as given in Algorithm 2. The mathematical model is based on hunting habits like prey search, persecution and jumping skills.

1) PERSECUTION PROCEDURE

The spider takes stealthy moves to come closer to the prey and sometimes jumps to catch the prey, known as the persecution strategy. The persecution strategy can be represented as

$$P_i = \frac{1}{2}at^2 + v_o t \quad (36)$$

P_i shows the current position of the spider, t represents time, and v_o is the initial velocity. The acceleration is indicated by

---

Algorithm 2 Jumping Spider Optimization

1: **procedure** JSOA
2: Define the objective function
3: Initialize the parameters of JSOA:
    Sea_Age, Max_Iter, a, Vo, φ
4: Initialize Spider positions
5: **while** *Iter < Max_Iter* **do**
6:    **if** *Rand_val < attack_or_search,* **then**
7:       **if** *Rand_val < p_attack,* **then**
8:          Perform the attack by persecution
9:       **else** Perform the attack by jumping on prey
10:      **end if**
11:   **else if** *Rand_val < q_search*
12:         Perform local search for prey
13:      **else** Perform global search for prey
14:      **end if**
15:   **end if**
16:   Update *Sea_Age* having low pheromone rates
17:   **if** fitness values with $P_{new} < P_{best}$, **then**
18:      $P_{best} = P_{new}$
19:   **end if**
20:   $Iter = Iter + 1$
21: **end while**
22: Show the optimal solution
23: **end procedure**

$a = \frac{v}{t}$, where $v = P - P_o$. The new position of the jumping spider is represented by

$$P_i(k+1) = \frac{1}{2}(P_i(k) - P_n(k)) \qquad (37)$$

where $P_i(k)$ is the current search position, $P_i(k+1)$ is the new search position, n is randomly generated between 1 and total number of spiders, $P_n(k)$ is the randomly selected spider with $i \neq n$.

2) JUMPING ON PREY

During hunting, the spider jumps on its prey. This movement resembles a projectile motion. The motion along x-axis can be represented as

$$P_i = v_o cos(\alpha)ti$$
$$\frac{dP}{dt} = V_P = V_o cos(\alpha)i \qquad (38)$$

The motion along y-axis can be represented as,

$$Q_i = \left(v_o sin(\alpha)t - \frac{1}{2}kt^2\right)j$$
$$\frac{dQ}{dt} = V_Q = (v_o sin(\alpha) - kt)j \qquad (39)$$

From (38) and (39), we arrive at the trajectory path representation, which is given by

$$Q = Ptan(\alpha) - \frac{kP^2}{2v_o^2cos^2(\alpha)} \qquad (40)$$

Finally, the new position $P_i(k+1)$ of the spider incorporating trajectory can be represented as

$$P_i(k+1) = P_i(k)\,tan(\alpha) - \frac{kP_i^2(k)}{2V_o^2cos^2(\alpha)}$$
$$\alpha = \frac{\phi\pi}{180} \qquad (41)$$

Here k represents gravity, and the angle α is calculated from randomly generated angle ϕ, where $\phi \in (0, 1)$.

3) SEARCHING FOR PREY

The spider roams around in its habitat and searches for prey. The prey search can be a local search or a global search.

The local search is given by

$$P_i(k+1) = P_{best}(k) + R\left(\frac{1}{2} - \psi\right) \qquad (42)$$

Here $P_i(k+1)$ is the new position of the spider, $P_{best}(k)$ is the best spider position from the previous iteration, $R \in (-2, 2)$ and $\psi \in (0, 1)$ are randomly generated numbers.

The global search is represented by

$$P_i(k+1) = P_{best}(k) + (P_{best}(k) - P_{worst}(k))\,C \qquad (43)$$

$P_i(k+1)$ represents the updated spider position, $P_{best}(k)$ is the best spider position, $P_{worst}(k)$ is the worst spider position, C is a random number following Cauchy distribution.

4) PHEROMONE RATE

The spiders release chemical substances called pheromones, causing behavioural changes. The pheromone rate is given by

$$Pheromone(i) = \frac{fitness_{max} - fitness_i}{fitness_{max} - fitness_{min}} \qquad (44)$$

Here $fitness_{min}$ indicates the best values of the objective function, $fitness_{max}$ indicates the worst values of the objective function, $fitness_i$ represents current value of objective function. From (44), spider positions with low pheromone rates are updated as

$$P_i(k) = P_{best}(k) + \frac{1}{2}\left[P_{n1}(k) - (-1)^{\sigma} * P_{n2}(k)\right] \qquad (45)$$

Here $P_i(k)$ represents spider with low pheromone rate, $n1$ and $n2$ are randomly generated between 1 and total number of spider population with $n1 \neq n2$, $P_{n1}(k)$ and $P_{n2}(k)$ are the selected spider agents, and $\sigma \in \{0, 1\}$ is a binary number randomly generated.

C. SOA APPROACH TOWARDS HPA LINEARIZATION

Seagulls are sea birds that utilise their intelligence to search and pound their prey. The SOA algorithm mimics seagull migration, and attacking behaviour is given in Algorithm 3.

1) MIGRATION

Seagulls perform a seasonal movement from one place to another in search of food. The SOA avoids collisions while

Algorithm 3 Seagull Optimization

1: **procedure** SOA
2: Define the objective function
3: Initialize the parameters of SOA:
    Sea_Age, *Max_Iter*, *A*, *B*, f_c, *u*, *v*
4: Initialize Seagull positions
5: **while** *Iter* < *Max_Iter* **do**
6:    Compute fitness function
7:    Start migration behaviour
8:    Generate random number r_d
9:    Generate random number *k*
10:    Start attacking behaviour
11:    Perform spiral behaviour
12:    Calculate distance
13:    Compute x, y, z planes
14   Save the best solution
15   Update Seagull positions
16:    *Iter* = *Iter* + 1
17: **end while**
18: Display the best solution
19: **end procedure**

Algorithm 4 Mexican Axolotl Optimization

1: **procedure** MAO
2: Define the objective function
3: Initialize the parameters of MAO:
    Sea_Age, *Max_Iter*, *Pop*, F_{Pop}, M_{Pop}, d_p, r_p, k, λ
4: Initialize Axolotl positions
5: **while** *Iter* < *Max_Iter* **do**
6:    Classify the population in to male M_{Pop}
        and female F_{Pop}
7:    Start transition procedure
8:    Select the best M_{Pop} and F_{Pop} based on
        objective function
9:    Inverse the probability of transition
10:    Update M_{Pop} and F_{Pop}
11:    Start Accidents procedure
12:    Perform regeneration process
13   Start new life procedure
14:    Perform assortment process
15:    Compute the value of objective function
16:    Select the best solution
17:    *Iter* = *Iter* + 1
18: **end while**
19: Show the best solution
20: **end procedure**

selecting the initial positions. The collision-free assignment of initial positions is ensured with (46).

$$C_i = U \times P_i(x) \qquad (46)$$

Here C_i represents the collision-free Seagull position or location, $P_i(x)$ is the present location of the Seagull, and x denotes the iteration number. The parameter U indicates the movement of the Seagull, which is given by

$$U = f - (x \times (f/Max\_Iter)) \qquad (47)$$

where $x = 0, 1, 2, \ldots, Max\_Iter$, Max_Iter represents the maximum number of iterations, f is a linearly decreasing variable used to specify the frequency of using the variable U. Once collision-free positions are allocated, Seagull moves towards the best neighbour's direction. This movement is represented as

$$M_i = E \times (P_{best}(x) - P_i(x)) \qquad (48)$$

M_i indicates the position of Seagull of P_i towards the best Seagull position, which is denoted by P_{best}, E is a balancing variable randomly calculated by (49).

$$E = 2 \times U^2 \times R_N \qquad (49)$$

where $R_N \in [0, 1]$ is a randomly generated number. Finally, in migration, the Seagull needs to update its position near to the best Seagull position. The position update is characterised as

$$D_i = |C_i + M_i| \qquad (50)$$

Here D_i represents the distance between the current Seagull position and the best Seagull position.

2) ATTACKING

The Seagull changes its altitude, speed and angle of attack according to the learning experience during the search process. While a seagull attacks prey, it performs a spiral movement. This movement along the x, y, and z planes is represented in (51)-(53).

$$M_x = r \times cos(\phi) \qquad (51)$$
$$M_y = r \times sin(\phi) \qquad (52)$$
$$M_z = r \times \phi \qquad (53)$$

r represents spiral radius as given in (54). ϕ in the range $[0 \leq \phi \leq 2\pi]$ is randomly generated.

$$r = a \times e^{\phi b} \qquad (54)$$

Here, a and b are spiral shape constants, and e represents the natural logarithm. Finally, the updated location of the Seagull with respect to the best seagull location is described as

$$p_i(x) = (D_i \times M_x \times M_y \times M_z) + P_{best}(x) \qquad (55)$$

Here $p_i(x)$ indicate the best solution.

D. MAO APPROACH TOWARDS HPA LINEARIZATION

The MAO algorithm that mimics the life of Axolotl is given in Algorithm 4. Axolotl is a Salamander seen in the lakes of Mexico city. The algorithm is motivated by the labour, reproduction, repair of tissues and behaviour of Axolotl in the aquatic environment.

1) TRANSITION FROM LARVAE TO ADULT

The total Axolotl population, $p(M, F)_j$ is divided into two subpopulations, namely male population M_j and female population F_j. Axolotl will adjust body part's colour towards male or female in the environment. Thus, Axolotl begins it's the transition from larvae to adult. The inverse probability calculation with male and female populations is given by

$$p(M, F)_j = \frac{obj(M_j, F_j)}{\sum obj(M_j, F_j)} \quad (56)$$

If the inverse probability of male axolotl is larger than the random value, then the male population needs to be updated.

$$M_{ji} = M_{ji} + (M_{best,i} - M_{ji}) * \gamma \quad (57)$$

M_{ji} represents male Axolotl, i represents the position, $M_{best,i}$ is the best-adapted male chosen by the best value of the objective function, and $\gamma \in [0, 1]$ represents the transition parameter. The male Axolotl can also do a random transition according to the optimization function.

$$M_{ji} = Min_i + (Max_i - Max_j) * R_i \quad (58)$$

$R_i \in [0, 1]$ is a randomly generated number, Min_i and Max_i represents the minimum and maximum dimension values of the of the objective function. Similarly, If the inverse probability of female axolotl is larger than the random value, then the female population needs to be updated.

$$F_{ji} = F_{ji} + F_{best,i} - F_{ji} * \gamma \quad (59)$$

F_{ji} represents female Axolotl, i represents the position, $F_{best,i}$ is the best-adapted female chosen by the best value of the objective function. The female Axolotl can also do a random transition according to the optimization function.

$$F_{ji} = Min_i + (Max_i - Max_j) * R_i \quad (60)$$

The above calculations update the best values of male and female Axolotls.

2) INJURY AND RESTORATION OF AXOLOTL

The Axolotls are prone to accidents and may develop injuries while moving into the water. Here, we need to perform the injury and restoration procedure. The process is described as

$$P_{ji} = Min_i + (Max_i - Min_i) * R_i \quad (61)$$

3) NEW LIFE PROCEDURE

For every male, a female is selected to produce offspring. The male axolotl produces spermatophores, and the female collects them. Here we assume every reproduction process involving a male and female axolotl contains two eggs. The newly formed individuals will compete with the parents after hatching. If the young returns the best value for the objective function, the parents are replaced by the young.

Algorithm 5 Black Widow Optimization

1: **procedure** BWOA
2: Define the objective function
3: Initialize the parameters of BWOA:
    $Sea\_Age, Max\_Iter, Rand\_val, \beta, m$
4: Initialize Spider positions
5: **while** $Iter < Max\_Iter$ **do**
6:     **if** $Rand\_val < 0.3$, **then**
7:         Perform the linear movement
8:     **else** Perform the spiral movement
9:     **end if**
10:     Calculate pheromone values of each agent
11:     Update Sea_Age having low pheromone rates
12:     Calculate P_{new}, fitness values of new agents
13:     **if** fitness values with $P_{new} < P_{best}$, **then**
14:         $P_{best} = P_{new}$
15:     **end if**
16:     $iter = ier + 1$
17: **end while**
18: Show the optimal solution
19: **end procedure**

E. BWOA APPROACH TOWARDS HPA LINEARIZATION

The BWOA, inspired by the movement and mating behaviour of black widow spiders, is given by Algorithm 5. These spiders are commonly seen in western parts of Canada and Southern regions of Mexico.

1) SPIDER MOVEMENT

The black widow shows both linear and spiral movements. This is represented by

$$P_i(t + 1) = \begin{cases} P_{best}(t) - m\, P_{n1}(t), & \text{if } rand() < 0.3, \\ P_{best}(t) - cos(2\pi\gamma)\, P_i(t), & \text{otherwise.} \end{cases}$$
$$(62)$$

Here $P_i(t + 1)$ represents the spider's updated position, $P_{best}(t)$ is the spider with best value from the last iteration, $m \in [0.4, 0.9]$ is a random number, n_1 is a random number generated between 1 and the maximum number of spiders, P_{n1} is the $n1^{th}$ search agent selected, with $i \neq n_1$, $\gamma \in [-1, 1]$ is randomly generated, and $P_i(t)$ represents the current spider position.

2) PHEROMONES

The pheromones play a major role in black widow mating behaviour. Sometimes, the female spider eats the male spider after or during mating to increase the chance of fertilization. So, the male spider chooses to avoid cannibalism and does not prefer a female spider with a low pheromone rate. The pheromone rate is given by

$$Pheromone(i) = \frac{fitness_{max} - fitness_i}{fitness_{max} - fitness_{min}} \quad (63)$$

TABLE 1. Simulation parameters and their values.

Simulation Parameter	Value
Modulation Order	4, 8, 16, 32
Sample rate	15.36 MHz
Amplifier Gain	55 dBm
Amplifier Saturation	52 dBm
Amplifier Input Power	-15 dBm to 30dBm
Memory Depth (Length)	3
Nonlinearity order (Degree)	7
Amplitude Imbalance	0.2 dB
Phase Imbalance	10

Here $fitness_{min}$ indicates the best values of the objective function, $fitness_{max}$ indicates the worst values of the objective function, $fitness_i$ represents current value of objective function. From (63), spider positions with low pheromone rates are updated as

$$P_i(t) = P_{best}(t) + \frac{1}{2}\left[P_{n1}(t) - (-1)^\lambda * P_{n2}(t)\right] \quad (64)$$

Here $P_i(t)$ represents spider with low pheromone rate, $n1$ and $n2$ are randomly generated between 1 and total number of spider population with $n1 \neq n2$, $P_{n1}(t)$ and $P_{n2}(t)$ are the selected spider agents, and $\lambda \in \{0, 1\}$ is a binary number randomly generated.

IV. RESULTS AND DISCUSSION

In this section, through the computer simulations, we analyze the impact of HPA in SWIPT. The parameters corresponding to baseband modulation, and HPA simulation is given in Table 1. The simulation is performed for 4, 8, 16, and 32-QAM schemes. The Amplifier Gain and Saturation are considered from Jang *et al.* [9], Amplifier Input power, Memory Depth (Length) and Non-linearity Order (Degree) are set based on Mukherjee *et al.* [16], and Amplitude and Phase Imbalance values are selected from Nair *et al.* [8].

Overall we consider PCE and RE analysis for evaluating the impact of DPD in SWIPT systems. Two types of DPD systems are applied to the transmitter side. The first is a conventional DPD system that finds the DPD coefficients through a least-squares solution. The second one is computing DPD coefficients through bio-inspired algorithms. A memory polynomial model characterizes the HPA with a standard LTE compliant signal and sampling rate of 15.36 MHz. The complex baseband IQ signals with IQ imbalance are loaded first into the power amplifier. Then the DPA coefficient matrix is determined using the least-squares solution of actual PA input data. The PCE and RE analysis is done at the receiver side. Then DPA is performed using adaptive bio-inspired algorithms, which showed improvement in the linearity of the SWIPT HPA transmitter. For both DPD methods, we analyze the PCE and RE with and without DPD assistance on the receiver side.

A. AM-AM AND AM-PM DISTORTION

The analysis of AM-AM distortion and AM-PM distortion in the transmitter section for the Ideal HPA and Practical HPA is
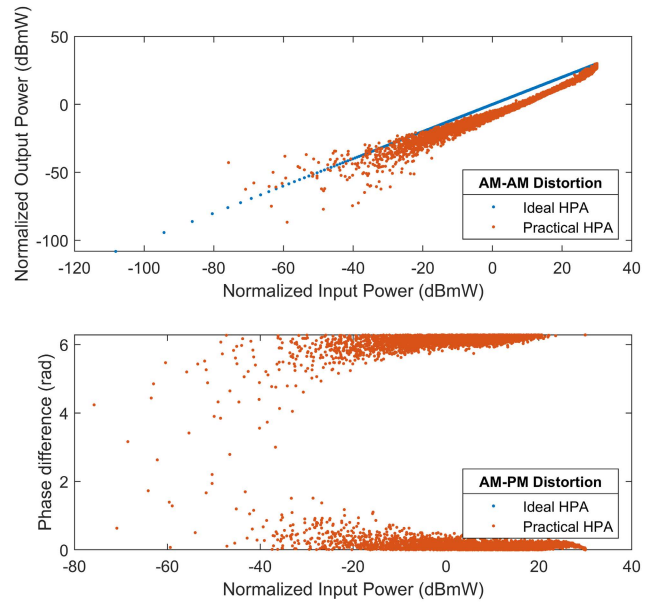

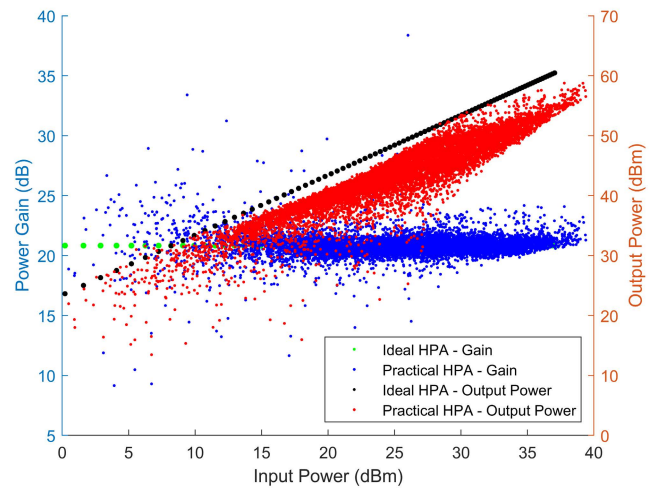**FIGURE 7.** AM-AM and AM-PM distortion in transmitter.

FIGURE 8. Power added efficiency comparison of HPA.

depicted in Figure 7. The ideal characteristic of HPA is linear, which is indicated by a straight line. But in a practical HPA case, the output increases nonlinearly due to compression when the amplifier's input level goes above the saturation point. The scattered points represent the memory effect. The memory effect occurs when the amplifier outputs depend on the current input and the signal at the previous instant. The graph would have contained only two straight lines representing instantaneous responses without memory effects. The memory effect further complicates the HPA problem. So, for the SWIPT transmitter, a practical HPA represented by the memory polynomial model is considered.

Further, Figure 8 depicts the behavioural difference between ideal HPA and practical HPA in standard parameters like gain, output power, and Power Added Efficiency (PAE). The most common parameter used to indicate high power amplifier efficiency is drain efficiency. But, a practical
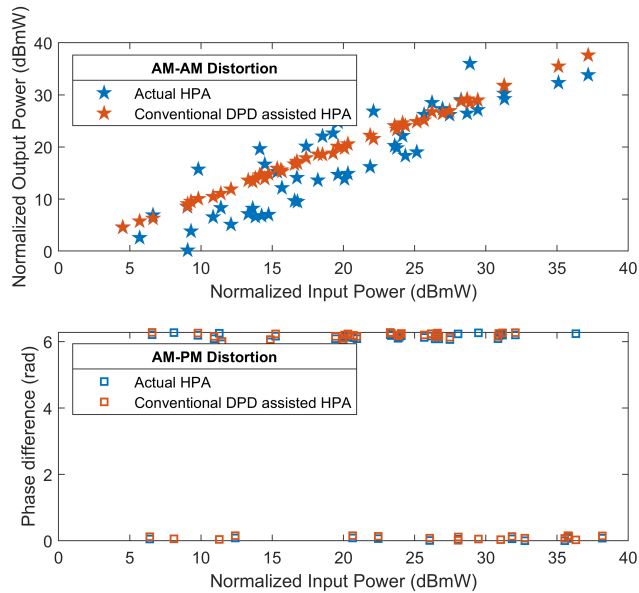
FIGURE 9. Performance of conventional DPD assisted HPA.

(a) DPD Disabled

(b) DPD Enabled

FIGURE 10. QAM constellation of the received signal.

HPA can deliver high drain efficiency with low gain. So, the PAE parameter is used here to analyze the amount of DC input power that contributes to power amplification. Unlike drain efficiency, the PAE shows the power utilized by the HPA. Thus the PAE characteristics also capture the nonlinear behaviour of HPA. So here, we apply DPD to linearize the HPA in the transmitter.

B. CONVENTIONAL DPD ASSISTED HPA

The DPD coefficients are extracted based on the memory depth and degree of the HPA polynomial model. Here the PA model is created based on half of the available PA dataset. The DPA distorts the signal before transmission by creating an inverse of the HPA characteristic. The linearity results of conventional DPD-assisted HPA are shown in Figure 9. The HPA characteristics with DPD approximate the ideal amplifier behaviour. Now the effect of DPD is analysed on the receiver side with the 16-QAM system as an example. At first, the data symbols are randomly generated. Then the signal is upsampled, and pulse shaping is performed using RRC with filter length $T = 10$ and roll-off factor $\alpha = 0.25$. The filtered signal is passed through the AWGN channel. The received signal is downsampled with the same oversampling factor and raised cosine filtering. The delay induced due to the filtering operation is also accounted for here. Now the received signal is demodulated, and symbols are recovered. The QAM constellation of the received signal with and without DPD is shown in Figure 10. The BER analysis with and without DPD assistance is given in Table 2. The Eb/No is set accordingly to obtain a BER rate in the 10^{-6} range. Due to nonlinearity, the BER rate increases as we move from the 4-QAM to the 16-QAM scheme. Consequently, EB/No has to be increased to keep BER in the 10^{-6} range. As observed from Table 2, with the help of DPD, the distortion caused by
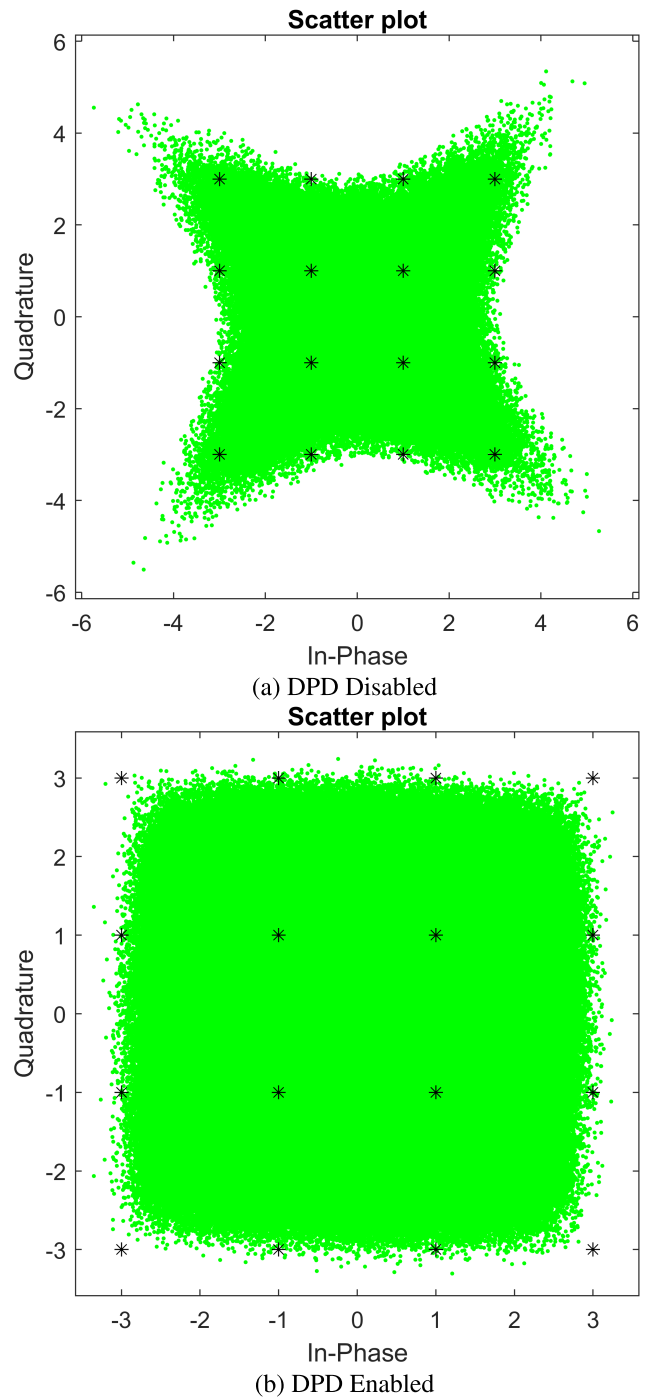
the PA is effectively removed. To understand the impact of DPD in energy harvesting, PCE is analysed with and without DPD assistance.

C. PCE ANALYSIS WITH CONVENTIONAL DPD

Figure 11 captures the impact of HPA nonlinearity on PCE. The PCE is also compared for different QAM schemes with and without the assistance of DPD in Table 3. The transmit

TABLE 2. BER values with and without DPD assistance.

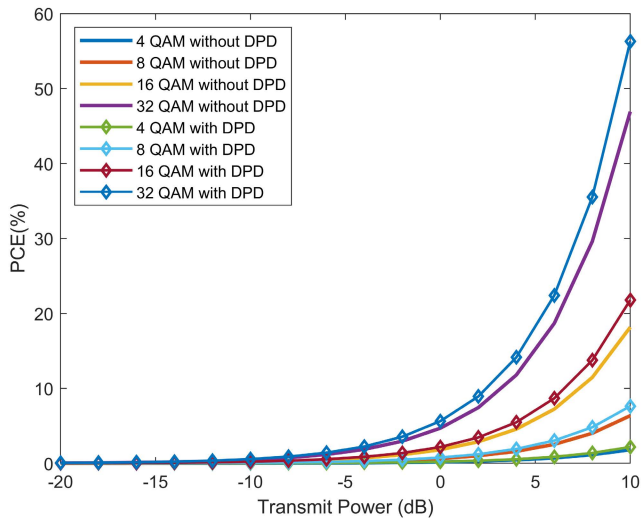| Modulation Scheme	BER without DPD	BER with Conventional DPD	Eb/No Required
4 QAM	4.67×10^{-6}	$\mathbf{4.67 \times 10^{-6}}$	10 dB
8 QAM	1.82×10^{-5}	$\mathbf{1.33 \times 10^{-6}}$	12 dB
16 QAM	3.30×10^{-5}	$\mathbf{9.81 \times 10^{-6}}$	16 dB
32 QAM	7.56×10^{-4}	$\mathbf{6.13 \times 10^{-6}}$	21 dB

FIGURE 11. Power conversion efficiency of SWIPT receiver.

TABLE 3. Power conversion efficiency.

Modulation Scheme	PCE without DPD	PCE with DPD	Improvement in PCE
4 QAM	2.03%	**2.27%**	**0.24%**
8 QAM	6.34%	**7.76%**	**1.42%**
16 QAM	18.16%	**22.16%**	**4.00%**
32 QAM	46.92%	**57.24%**	**10.32%**

power is set from -20 dB to 10 dB. The minimum transmit power required for energy harvesting is -8dB. We observe that PCE increases from 4-QAM to the 32-QAM scheme. A maximum PCE of 57.24% is obtained for the 32 QAM scheme with DPD. Also, PCE is improved by 10.32% compared with 32 QAM without DPD assistance. The DPD showed improvement of about 4% for 16QAM, 1.42% for 8QAM, and 0.24% for 4 QAM. The compromise between harvested energy and information rate for a conventional DPD-assisted SWIPT system is visualized through the RE region.

D. RE ANALYSIS WITH CONVENTIONAL DPD
The RE region analysis sets bounds and limits the overall performance of the SWIPT PS system as expressed in (29). We consider the same transmission power and efficiency as discussed in the previous section. The power splitting ratio ρ is varied between 0 and 1. All the symbols are assumed to have unit power. The complex AWGN produced during power splitting is considered to have zero mean and
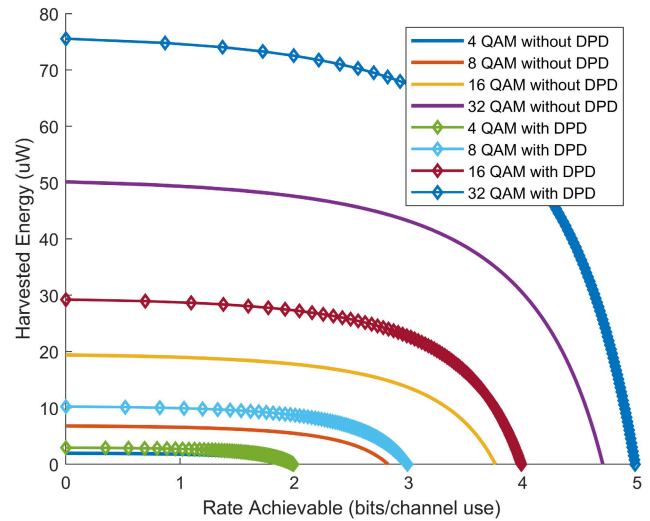

FIGURE 12. Rate energy region of SWIPT receiver.

TABLE 4. Rate energy for conventional DPD.

	Modulation	Max Energy	Max Rate	Energy when $\rho = 0.5$	Rate when $\rho = 0.5$
Without DPD	4 QAM	1.94	1.92	0.97	1.68
	8 QAM	6.79	2.82	3.39	2.52
	16 QAM	19.41	3.76	9.70	3.36
	32 QAM	50.14	4.7	25.06	4.2
With DPD	4 QAM	**2.92**	**1.99**	**1.46**	**1.78**
	8 QAM	**10.23**	**2.98**	**5.11**	**2.67**
	16 QAM	**29.23**	**3.97**	**14.61**	**3.56**
	32 QAM	**75.5**	**4.96**	**37.75**	**4.45**

variance $2\sigma^2$. The complex AWGN encompasses noise due to antenna and processing of data. The rate energy for conventional DPD is given in Table 4.

E. BIO-INSPIRED DPD ASSISTED HPA
The bio-inspired algorithm-based DPD is adopted for HPA linearization. The HPA assumes the same memory polynomial model. The parameters and values used in the bio-inspired algorithms are given in Table 5. The combination of bio-inspired pre-distorter and HPA produces linear characteristics, which are portrayed in Figure 13. This linearity is exhibited till the point of saturation of HPA. To compare the performance of bio-inspired DPD assisted HPA with the conventional DPD assisted HPA, and the same 16-QAM scheme is selected.

In Table 6, the linearity and performance of the bio-inspired DPD are compared using metrics, namely Fisher Discriminant Ratio (FDR), Mean of Slope (MS), and Mean of Phase Difference (MPD).

The BER values for bio-inspired DPD-assisted SWIPT are provided in Table 7. The BER analysis is performed with the same Eb/No value as in the conventional DPD case. Among all the bio-inspired algorithms, the SOA performs better for the 16-QAM scheme. The metrics indicated in Table 6

TABLE 5. Algorithm parameters.

DOA	JSOA	SOA	MAO	BWOA
Sea_Age=100	Sea_Age=100	Sea_Age=100	Sea_Age=100	Sea_Age=100
Max_iter=100	Max_iter=100	Max_iter=100	Max_iter=100	Max_iter=100
$P_{hunt} = 0.5$	$a = 9.80665$	$R_N \in [0, 1]$	$\gamma \in [0, 1]$	$\beta \in (-1, 1)$
$Q_{attack} = 0.7$	$v_0 = 100$	$\phi \in [0, 2\pi]$	$R_i \in [0, 1]$	$m \in (0.4, 0.9)$
$\beta_1 \in [-2, 2]$	$\phi \in [0, 1]$	-	-	-
$\beta_2 \in [-1, 1]$	-	-	-	-

TABLE 6. Comparison metrics for HPA linearization.

Metric	DOA	JSOA	SOA	MAO	BWOA	Conventional DPD
FDR	0.18	0.10	**0.05**	0.02	0.06	0.14
MS	-0.00108	-0.00112	**-9.943**	-8.824	-8.934	-0.00105
MPD	6.14	6.05	**5.56**	6.18	6.17	4.72

Note: FDR is used to find out the inter-cluster and intra-cluster distance in data points. Slope gives the rate of change of output with respect to input. Phase difference is calculated as the difference in phase between actual HPA and linearized HPA.

TABLE 7. BER values for bio-inspired DPD assisted SWIPT.

Modulation Scheme	DOA	JSOA	SOA	MAO	BWOA	Eb/No Required
4-QAM	4.67×10^{-6}	$4.00 \times 10-6$	$\mathbf{2.67 \times 10-6}$	2.67×10^{-6}	$3.33 \times 10-6$	10 dB
8-QAM	3.56×10^{-6}	1.78×10^{-6}	$\mathbf{8.89 \times 10^{-7}}$	8.89×10^{-7}	4.44×10^{-7}	12 dB
16-QAM	2.57×10^{-5}	8.67×10^{-6}	$\mathbf{2.33 \times 10^{-6}}$	3.00×10^{-6}	4.00×10^{-6}	16 dB
32-QAM	$6.29 \times 10-5$	1.41×10^{-5}	$\mathbf{1.33 \times 10^{-6}}$	1.60×10^{-6}	5.60×10^{-6}	21 dB

TABLE 8. BER comparison of conventional and bio-inspired DPD.

Modulation Scheme	DOA	JSOA	SOA	MAO	BWOA
4-QAM	0	$6.70 \times 10-7$	$\mathbf{2.00 \times 10-6}$	2.00×10^{-6}	$1.34 \times 10-6$
8-QAM	-2.23×10^{-6}	-4.50×10^{-7}	$\mathbf{4.41 \times 10^{-7}}$	4.41×10^{-7}	8.86×10^{-7}
16-QAM	-1.59×10^{-5}	1.14×10^{-6}	$\mathbf{7.48 \times 10^{-6}}$	6.81×10^{-6}	5.81×10^{-6}
32-QAM	$-5.68 \times 10-5$	-7.97×10^{-6}	$\mathbf{4.80 \times 10^{-6}}$	4.53×10^{-6}	5.30×10^{-7}
Arithmetic Mean	$\mathbf{-1.87 \times 10-5}$	$\mathbf{-1.65 \times 10^{-6}}$	$\mathbf{3.68 \times 10^{-6}}$	$\mathbf{3.45 \times 10^{-6}}$	$\mathbf{2.14 \times 10^{-6}}$

Note:The Table provides the mean difference in BER value for Conventional DPD and Bio-inspired DPD for different QAM schemes. The negative value of DOA and JSOA signifies the increase in the error rate, and the positive values of SOA, MAO and BWOA indicate the reduction in the error rate.

interpret this performance. The SOA has $FDA \leq 0.06$ with the least slope and MPD value in $5.5 < MPD < 6.28$. Similarly, the underperformance of DOA compared to conventional DPD can also be visualized. But, in the case of DOA, the PCE and harvested energy are better than conventional DPD, which is discussed in the next section.

F. PCE ANALYSIS WITH BIO-INSPIRED DPD
The PCE analysis for bio-inspired DPD is given in Figure 14, and Table 9 provides the comparison with conventional DPD. Here DOA performs the best when compared with all other bio-inspired algorithms. Since the BER value of DOA is slightly more than conventional DPD, we conclude that the increase in PCE of DOA is due to the erroneous bits. To emphasise this point, if we observe the PCE of the 32-QAM scheme, DOA has a considerable increase in maximum PCE of 77.11%. This increase is 6.23% more than the JSOA, which comes next in the 32-QAM PCE category. The PCE value for MAO appears to be the least compared

to all the other bio-inspired algorithms but holds a better BER rate, as discussed in the previous section. If we look for a fair BER rate and aim to harvest a reasonable amount of energy simultaneously, SOA would be the best option. Here, RE analysis gives a better picture of the simultaneous transmission of energy and information. Here, RE analysis provides a better view of the simultaneous transmission.

G. RE ANALYSIS WITH BIO-INSPIRED DPD
The rate energy analysis for bio-inspired DPD-assisted HPA is given in Figure 15, and Table 10 provides the maximum energy and maximum rate achieved for different user scenarios. The results show that DOA performs the best among all three users. The maximum energy of 12 μW is obtained for DOA under the 32-QAM scheme. Here the harvested energy is 18.94 μW more when compared to JSOA under the same 32-QAM scheme. But, as discussed previously, this improvement in harvested energy and information rate is due to the erroneously received bits. For a SWIPT user employing a

TABLE 9. Power conversion efficiency for bio-inspired algorithms.

	4-QAM		8-QAM	
Bio-inspired Algorithm	Maximum PCE	PCE improvement compared to conventional DPD	Maximum PCE	PCE improvement compared to conventional DPD
DOA	**3.73%**	**1.46%**	**13.05%**	**5.29%**
JSOA	3.42%	1.15%	11.99%	4.23%
SOA	3.08%	0.81%	10.78%	3.02%
MAO	2.89%	0.62%	10.13%	2.37%
BWOA	3.17%	0.90%	11.10%	3.34%
	16-QAM		32-QAM	
DOA	**29.84%**	**7.68%**	**77.11%**	**19.87%**
JSOA	27.42%	5.26%	70.85%	13.61%
SOA	24.65%	2.49%	63.69%	6.45%
MAO	23.17%	1.01%	59.86%	2.62%
BWOA	25.38%	3.22%	65.58%	8.34%

TABLE 10. Rate energy for bio-inspired algorithm based DPD.

|	4-QAM				8-QAM			
Bio-inspired Algorithm	Maximum Energy	Maximum Rate	Energy when $\rho=0.5$	Rate when $\rho=0.5$	Maximum Energy	Maximum Rate	Energy when $\rho=0.5$	Rate when $\rho=0.5$
DOA	**4.71**	**1.97**	**2.30**	**1.72**	**16.49**	**2.95**	**8.08**	**2.58**
JSOA	3.97	1.91	1.94	1.66	13.92	2.87	6.82	2.50
SOA	3.21	1.85	1.57	1.60	11.25	2.77	5.51	2.40
MAO	2.84	1.81	1.39	1.56	9.94	2.72	4.87	2.34
BWOA	3.40	1.87	1.67	1.62	11.93	2.80	5.84	2.43
	16-QAM				32-QAM			
DOA	**47.12**	**3.94**	**23.09**	**3.44**	**121.73**	**4.92**	**59.65**	**4.30**
JSOA	39.79	3.83	19.49	3.33	102.79	4.79	50.36	4.17
SOA	32.15	3.70	15.75	3.20	83.05	4.63	40.69	4.00
MAO	28.40	3.62	13.91	3.13	73.38	4.53	35.95	3.91
BWOA	34.08	3.74	16.70	3.24	88.06	4.67	43.15	4.05

Note: The maximum energy and maximum rate represent Idle and Active users, respectively. The information rate for the Idle user is zero. Similarly, the harvested energy for the Active user is zero. For the SWIPT user, energy and information rate are simultaneously achieved considering the PS ratio, $\rho = 0.5$.

**TABLE 11.** Comparison of rate-energy with existing benchmark literature works.

Year	Author	Work	4-QAM		8-QAM		16-QAM		32-QAM	
			Maximum Energy	Maximum Rate	Maximum Energy	Maximum Rate	Maximum Energy	Maximum Rate	Maximum Energy	Maximum Rate
2013	Zhang et al. [48]	MIMO for SWIPT system	**225**	**2**	**220**	**3**	**205**	**4**	**180**	**5**
2013	Liu et al. [49]	Dynamic PS in SWIPT	5..95	2	5.9	3	5.8	4	5.65	5
2014	Huang et al. [50]	SWIPT with OFDMA	11.2	2	10.6	3	9.4	4	7.9	5
2018	Clerckx et al. [51]	SWIPT with Nonlinearities	10	2	7.5	3	5.6	4	2.5	5
2020	Li et al. [52]	Full-Duplex SWIPT System	3.2	2	3.1	3	2.9	4	2.5	5
This Work	Nair et al.	Nature inspired DPD assisted SWIPT	4.71	1.97	16.49	2.95	47.12	3.94	121.73	4.92

32-QAM scheme, the MAO, SOA, and BWOA give a maximum information rate of 4.53, 4.63 and 4.67 bits/channel use. The maximum harvested energy yielded for the SWIPT user using the above algorithms is obtained as 35.95, 40.69 and 43.15 μW respectively. A comparison between the bio-inspired approach and the existing benchmark literature works is given in Table 11. The results are compared for an SNR value of 20dB. The harvested energy in the proposed work increases from $4.71\mu W$ to $121.73\mu W$ when we move from 4-QAM to the 32-QAM scheme but maintain a fair information rate. On the other hand, the trend of benchmark schemes is that the harvested energy decreases when we move from 4-QAM to the 32-QAM scheme. The reason is that in the proposed work, the bio-inspired algorithm focuses more on energy harvesting by maintaining a fair information rate close to the benchmark schemes.
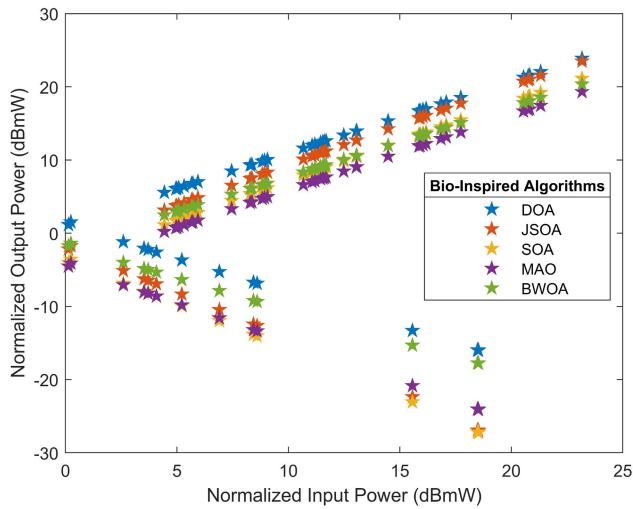
(a) AM-AM Distortion after applying Bio-inspired DPD
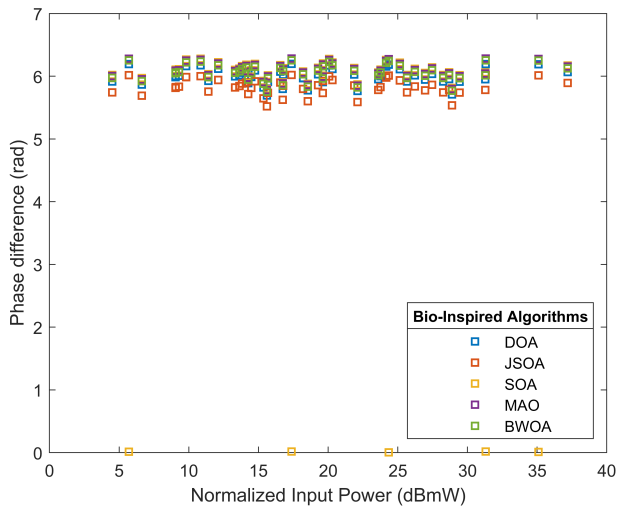
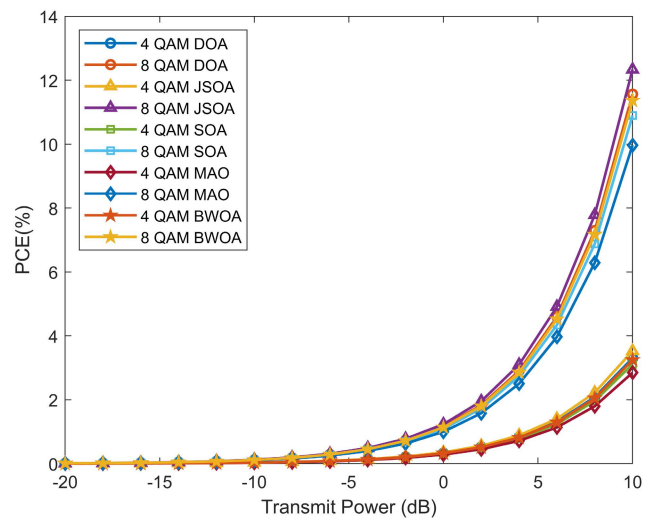(b) AM-PM Distortion after applying Bio-inspired DPD

FIGURE 13. Performance of Bio-inspired DPD assisted HPA.
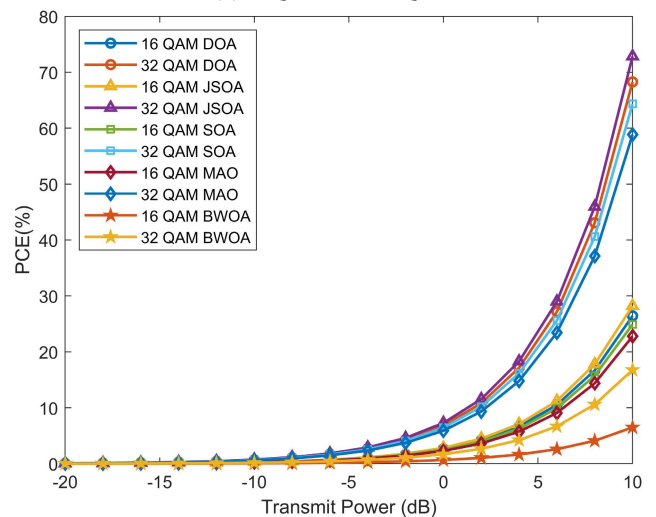
TABLE 12. Computational complexity of bio-inspired algorithms.

Bio-Inspired Algorithm	Computational Complexity
DOA	$\mathcal{O}(n \log 2n)$
JSOA	$\mathcal{O}(n^2 \log 2n)$
SOA	$\mathcal{O}(n \log 4n)$
MAO	$\mathcal{O}(n \log 4n)$
BWOA	$\mathcal{O}(n \log 4n)$

H. COMPUTATIONAL COMPLEXITY

The computation complexity of the bio-inspired algorithms is calculated with the input size n. For example, if we denote $\mathcal{O}(\log n)$, then it conveys that computational complexity increases $\log(n)$ times for any increase in 'n'. Table 12 shows that DOA has the least computational complexity of $\mathcal{O}(n \log 2n)$. The complexity value substantiates the increase in BER and PCE for the DOA algorithm. Similarly, JSOA was unable to perform well because of high computational complexity $\mathcal{O}(n^2 \log 2n)$ compared to other algorithms. The SOA,

(a) 4 QAM and 8 QAM

(b) 16 QAM and 32 QAM

FIGURE 14. Power conversion efficiency of SWIPT receiver after applying Bio-inspired DPD.

MAO and BWOA have the same computational complexity of $\mathcal{O}(n \log 4n)$, and these algorithms attained closer results in BER, PCE and RE analysis.

I. COMPARISON WITH PREVIOUS WORK

Table 13 compares our work with existing SWIPT energy harvesting models. The maximum harvested energy obtained in the existing articles is converted to dBmW for a fair comparison. As discussed at the beginning of this section, the conventional DPD uses the least-squares algorithm to eliminate the nonlinearity present in HPA. The least-square algorithm that works on model fitting minimizes the difference between the input and output of HPA are skewed with initial and extreme values. Although the least-square algorithm works well in typical wireless communication systems, it lacks performance in a dynamic scenario like the SWIPT system, which focuses simultaneously on energy harvesting

TABLE 13. Comparison with previous work on SWIPT based Energy Harvesting.

Year	Author	Work	Maximum Harvested Energy
2022	Nair et.al [8]	Harvested energy maximization for SWIPT with IQ imbalance hardware impairment	41 dBmW (50 dBmW*) for 32-QAM
2020	Chien et.al [53]	Harvested energy and BER optimization for SWIPT using sadde	51 dBmW (70 dBmW*) BER = 1×10^{-6}
2020	Mukherjee et.al [16]	MIMO enabled SWIPT system with power amplifier nonlinearities	-5 dBmW (14 dBmW*)
2019	Xu et.al [54]	Nonlinear energy harvesting based SWIPT for MIMO system	-16 dBmW (18 dBmW*)
2019	Li et.al [55]	Information rate and harvested energy for SWIPT with non-linear energy harvesting	42 dBmW (50 dBmW*)
2019	Peng and Lee [56]	Energy harvesting maximization for SWIPT using popularity cache scheme	-9 dBmW (30 dBmW*)
2018	Morsi et.al [57]	Energy harvesting in SWIPT using separate receiver circuit	-24 dBmW (54 dBmW*)
2018	Lu et.al [58]	Nonlinear energy harvesting based SWIPT for MISO system	14 dBmW (36 dBmW*)
This Work	Nair et.al	Nature inspired DPD assisted SWIPT with nonlinearities	-12 dBmW (40 dBmW*) for 32-QAM BER = 1.33×10^{-6}

Note: * denotes transmit Power

(a) 4 QAM and 8 QAM
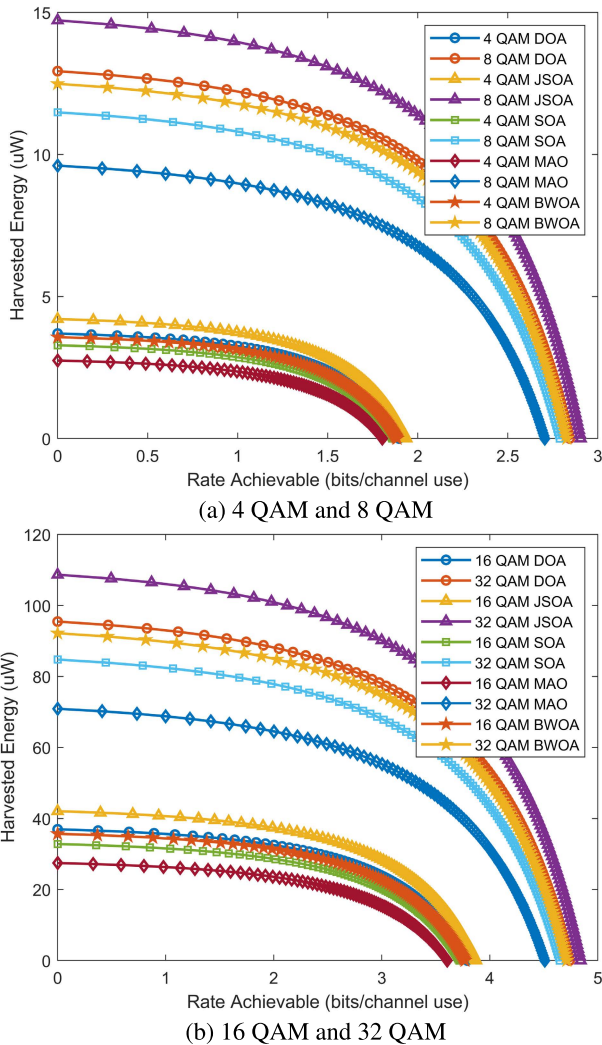

(b) 16 QAM and 32 QAM

FIGURE 15. Rate energy region of SWIPT receiver after applying Bio-inspired DPD.

and information rate. Also, depending on the demand for harvested energy, the SWIPT system must switch between the modulation scheme accordingly.

V. CONCLUSION

The SWIPT enables the wireless networks to transfer energy and information simultaneously. The significant problem faced by the SWIPT system during practical implementation is hardware impairment. The hardware impairment assumed in this work is the combined effect of In-phase and Quadrature imbalance and High Power Amplifier nonlinearity. A DPD-assisted M-ary modulated SWIPT transmitter is considered to compensate for the nonlinearity caused due to hardware impairments. Compared with SWIPT without DPD, the conventional DPD-assisted SWIPT harvested maximum energy of 25.06 μW and exhibited a maximum improvement of 10.32% in PCE under the 32-QAM scheme keeping the BER rate in the range of 10^{-6}. Then conventional DPD is replaced with bio-inspired algorithms such as Dingo Optimization, Jumping Spider Optimization, Seagull Optimization, Mexican Axolotl Optimization, and Black Widow Optimization. Among the various bio-inspired algorithms Seagull Optimisation algorithm harvested maximum energy of 35.95 μW and showed a maximum improvement of 6.45% in PCE compared to conventional DPD. The limitation of using bio-inspired DPD is the increase in complexity and hardware cost of the system. The recommended future direction of the work is to use other bio-inspired algorithms to improve PCE and harvested energy by keeping a fair bit error rate. Practical HPA with memory effects can be modelled through bio-inspired algorithms based on the optimal design to reflect the ideal power and gain characteristics of the amplifier. Also, the SWIPT system can be modelled and visualised in a co-existing multi-user environment.

REFERENCES

[1] W. Lu, P. Si, G. Huang, H. Han, L. Qian, N. Zhao, and Y. Gong, "SWIPT cooperative spectrum sharing for 6G-enabled cognitive IoT network," *IEEE Internet Things J.*, vol. 8, no. 20, pp. 15070–15080, Oct. 2021.

[2] L. R. Varshney, "Transporting information and energy simultaneously," in *Proc. IEEE Int. Symp. Inf. Theory*, Jul. 2008, pp. 1612–1616.

[3] J.-M. Kang, I.-M. Kim, and D. I. Kim, "Wireless information and power transfer: Rate-energy tradeoff for nonlinear energy harvesting," *IEEE Trans. Wireless Commun.*, vol. 17, no. 3, pp. 1966–1981, Mar. 2018.

[4] T. D. P. Perera, D. N. K. Jayakody, S. Chatzinotas, and J. Li, "Simultaneous wireless information and power transfer (SWIPT): Recent advances and future challenges," *IEEE Commun. Surveys Tuts.*, vol. 20, no. 1, pp. 264–302, 1st Quart., 2018.

[5] T. Schenk, *RF Imperfections in High-Rate Wireless Systems: Impact and Digital Compensation*. Dordrecht, The Netherlands: Springer, 2008.

[6] H. Tsou, "The effect of phase and amplitude imbalance on the performance of offset quadrature phase-shift-keyed (OQPSK) communication systems," *Telecommun. Mission Oper. Prog. Rep.*, vol. 135, pp. 1–15, Jul. 1998.

[7] A. R. Nair, S. Kirthiga, and M. Jayakumar, "Estimation and compensation of IQ imbalance in SWIPT system," *Int. J. Electron. Telecommun.*, vol. 67, no. 4, pp. 679–684, 2021.

[8] A. R. Nair and S. Kirthiga, "Analysis of energy harvesting in SWIPT using bio-inspired algorithms," *Int. J. Electron.*, vol. 2022, pp. 1–21, Feb. 2022.

[9] H. H. Jang, K. W. Choi, and D. I. Kim, "Novel frequency-splitting SWIPT for overcoming amplifier nonlinearity," *IEEE Wireless Commun. Lett.*, vol. 9, no. 6, pp. 826–829, Jun. 2020.

[10] A. R. Nair and S. Kirthiga, "Impact of total harmonic distortion in SWIPT enabled wireless communication networks," in *Proc. Smart Technol., Commun. Robot. (STCR)*, Oct. 2021, pp. 1–5.

[11] J. J. Park, J. H. Moon, H. H. Jang, and D. I. Kim, "Performance analysis of power amplifier nonlinearity on multi-tone SWIPT," *IEEE Wireless Commun. Lett.*, vol. 10, no. 4, pp. 765–769, Apr. 2021.

[12] W. Liu, X. Zhou, S. Durrani, and P. Popovski, "SWIPT with practical modulation and RF energy harvesting sensitivity," in *Proc. IEEE Int. Conf. Commun. (ICC)*, May 2016, pp. 1–7.

[13] L. Chen, X. Wu, X. Wang, W. Qi, X. Hong, J. Shi, J. Hu, and K. Yang, "Performance tradeoff analysis of hybrid signaling SWIPT systems with nonlinear power amplifiers," *Electronics*, vol. 10, no. 11, p. 1364, 2021.

[14] J. Sun, W. Shi, Z. Yang, J. Yang, and G. Gui, "Behavioral modeling and linearization of wideband RF power amplifiers using BiLSTM networks for 5G wireless systems," *IEEE Trans. Veh. Technol.*, vol. 68, no. 11, pp. 10348–10356, Nov. 2019.

[15] Z. A. Khan, E. Zenteno, P. Händel, and M. Isaksson, "Digital predistortion for joint mitigation of I/Q imbalance and MIMO power amplifier distortion," *IEEE Trans. Microw. Theory Techn.*, vol. 65, no. 1, pp. 322–333, Jan. 2017.

[16] P. Mukherjee, S. Lajnef, and I. Krikidis, "MIMO SWIPT systems with power amplifier nonlinearities and memory effects," *IEEE Wireless Commun. Lett.*, vol. 9, no. 12, pp. 2187–2191, Dec. 2020.

[17] G. Negi, A. Kumar, S. Pant, and M. Ram, "Optimization of complex system reliability using hybrid grey wolf optimizer," *Decis. Making, Appl. Manage. Eng.*, vol. 4, no. 2, pp. 241–256, 2021.

[18] L. dos Santos Coelho and V. C. Mariani, "Use of chaotic sequences in a biologically inspired algorithm for engineering design optimization," *Expert Syst. Appl.*, vol. 34, no. 3, pp. 1905–1913, 2008.

[19] R. C. T. de Souza, C. A. de Macedo, L. dos Santos Coelho, J. Pierezan, and C. V. Mariani, "Binary coyote optimization algorithm for feature selection," *Pattern Recognit.*, vol. 107, Nov. 2020, Art. no. 107470.

[20] A. H. Abdelhafiz, O. Hammi, A. Zerguine, A. T. Al-Awami, and F. M. Ghannouchi, "A PSO based memory polynomial predistorter with embedded dimension estimation," *IEEE Trans. Broadcast.*, vol. 59, no. 4, pp. 665–673, Dec. 2013.

[21] P. Bipin and P. Rao, "Linearization of high power amplifier using modified artificial bee colony and particle swarm optimization algorithm," *Proc. Technol.*, vol. 25, pp. 28–35, Jan. 2016.

[22] S. Wang, "Study on complexity reduction of digital predistortion for power amplifier linearization," Ph.D. dissertation, School Math., Sci. Technol. Inf. Commun., Paris-Est Univ., Champs-sur-Marne, France, 2018.

[23] W. A. Tsou, W. S. Wuen, T. Y. Yang, and K. A. Wen, "Analysis and compensation of the AM-AM and AM-PM distortion for CMOS cascode class-E power amplifier," *Int. J. Microw. Sci. Technol.*, vol. 2009, pp. 1–10, Mar. 2009.

[24] C. Paoloni, D. Gamzina, R. Letizia, Y. Zheng, and N. C. Luhmann, Jr., "Millimeter wave traveling wave tubes for the 21st century," *J. Electromagn. Waves Appl.*, vol. 35, no. 5, pp. 567–603, Dec. 2020.

[25] N. Khalfet and I. Krikidis, "Information energy capacity region for SWIPT systems over Rayleigh-fading channels," *IEEE Trans. Commun.*, early access, May 12, 2022, doi: 10.1109/TCOMM.2022.3174068.

[26] J. Kim and K. Konstantinou, "Digital predistortion of wideband signals based on power amplifier model with memory," *Electron. Lett.*, vol. 37, no. 23, pp. 1417–1418, Nov. 2001.

[27] C. Huang, S. Zhou, J. Xu, Z. Niu, R. Zhang, and S. Cui, *Energy Harvesting Wireless Communications*. Hoboken, NJ, USA: Wiley, 2018.

[28] G. Vieeralingaam, R. Ramanathan, and M. Jayakumar, "Convex optimization approach to joint interference and distortion minimization in energy harvesting wireless sensor networks," *Arabian J. Sci. Eng.*, vol. 45, no. 3, pp. 1669–1684, Mar. 2020.

[29] G. Vieeralingaam and R. Ramanathan, "Parametric study of RF energy harvesting in SWIPT enabled wireless networks under downlink scenario," *Proc. Comput. Sci.*, vol. 143, pp. 835–842, Jan. 2018.

[30] M. Sundaram and R. Ramanathan, "Performance optimization of RF energy harvesting wireless sensor networks," *Proc. Comput. Sci.*, vol. 115, pp. 831–837, Jan. 2017.

[31] H. Peraza-Vázquez, A. F. Peña-Delgado, G. Echavarría-Castillo, A. B. Morales-Cepeda, J. Velasco-Álvarez, and F. Ruiz-Perez, "A bio-inspired method for engineering design optimization inspired by dingoes hunting strategies," *Math. Problems Eng.*, vol. 2021, pp. 1–19, Sep. 2021.

[32] H. Peraza-Vázquez, A. Peña-Delgado, P. Ranjan, C. Barde, A. Choubey, and A. B. Morales-Cepeda, "A bio-inspired method for mathematical optimization inspired by Arachnida Salticidae," *Mathematics*, vol. 10, no. 1, pp. 102–134, 2022.

[33] G. Dhiman and V. Kumar, "Seagull optimization algorithm: Theory and its applications for large-scale industrial engineering problems," *Knowl.-Based Syst.*, vol. 165, pp. 169–196, Feb. 2018.

[34] Y. Villuendas-Rey, J. L. Velázquez-Rodríguez, M. D. Alanis-Tamez, M.-A. Moreno-Ibarra, and C. Yáñez-Márquez, "Mexican axolotl optimization: A novel bioinspired heuristic," *Mathematics*, vol. 9, no. 7, pp. 781–801, 2021.

[35] A. F. Peña-Delgado, H. Peraza-Vázquez, J. H. Almazán-Covarrubias, N. T. Cruz, P. M. García-Vite, A. B. Morales-Cepeda, and J. M. Ramirez-Arredondo, "A novel bio-inspired algorithm applied to selective harmonic elimination in a three-phase eleven-level inverter," *Math. Problems Eng.*, vol. 2020, pp. 1–10, Dec. 2020.

[36] L. Najafizadeh and C. Tellambura, "BER analysis of arbitrary QAM for MRC diversity with imperfect channel estimation in generalized Ricean fading channels," *IEEE Trans. Veh. Technol.*, vol. 55, no. 4, pp. 1239–1248, Jul. 2006.

[37] M. Schetzen, *The Volterra and Wiener Theories of Nonlinear Systems*. Hoboken, NJ, USA: Wiley, 1980.

[38] G. M. Raz and B. D. Van Veen, "Baseband Volterra filters for implementing carrier based nonlinearities," *IEEE Trans. Signal Process.*, vol. 46, no. 1, pp. 103–114, Jan. 1998.

[39] A. E. Nordsjo and L. H. Zetterberg, "Identification of certain time-varying nonlinear Wiener and Hammerstein systems," *IEEE Trans. Signal Process.*, vol. 49, no. 3, pp. 577–592, Mar. 2001.

[40] H. W. Kang, Y. S. Cho, and D. H. Youn, "Adaptive precompensation of Wiener systems," *IEEE Trans. Signal Process.*, vol. 46, no. 10, pp. 2825–2829, Oct. 1998.

[41] J. K. Cavers, "The effect of quadrature modulator and demodulator errors on adaptive digital predistorters for amplifier linearization," *IEEE Trans. Veh. Technol.*, vol. 46, no. 2, pp. 456–466, May 1997.

[42] J. D. Gibson, *Principles of Analog and Digital Communications*, 2nd ed. Upper Saddle River, NJ, USA: Prentice-Hall, 1993.

[43] P. P. Campo, L. Anttila, D. Korpi, and M. Valkama, "Cascaded spline-based models for complex nonlinear systems: Methods and applications," *IEEE Trans. Signal Process.*, vol. 69, pp. 370–384, 2020.

[44] M. Cansiz, D. Altinel, and G. K. Kurt, "Efficiency in RF energy harvesting systems: A comprehensive review," *Energy*, vol. 174, pp. 292–309, May 2019.

[45] R. Perez, *Wireless Communications Design Handbook: Interference Into Circuits: Aspects of Noise, Interference, and Environmental Concerns*. New York, NY, USA: Academic, 1998.

[46] M. Bonnin, F. L. Traversa, and F. Bonani, "Leveraging circuit theory and nonlinear dynamics for the efficiency improvement of energy harvesting," *Nonlinear Dyn.*, vol. 104, no. 1, pp. 367–382, 2021.

[47] R. Zhang and C. K. Ho, "MIMO broadcasting for simultaneous wireless information and power transfer," *IEEE Trans. Wireless Commun.*, vol. 12, no. 5, pp. 1989–2001, May 2013.

[48] L. Liu, R. Zhang, and K.-C. Chua, "Wireless information and power transfer: A dynamic power splitting approach," *IEEE Trans. Commun.*, vol. 61, no. 9, pp. 3990–4001, Sep. 2013.

[49] K. Huang and E. Larsson, "Simultaneous information and power transfer for broadband wireless systems," *IEEE Trans. Signal Process.*, vol. 61, no. 23, pp. 5972–5986, Dec. 2013.

[50] B. Clerckx, "Wireless information and power transfer: Nonlinearity, waveform design, and rate-energy tradeoff," *IEEE Trans. Signal Process.*, vol. 66, no. 4, pp. 847–862, Feb. 2018.

[51] M. Li, X. Tao, N. Li, and H. Wu, "Multi-objective optimization for full-duplex SWIPT systems," *IEEE Access*, vol. 8, pp. 30838–30853, 2020.

[52] W. Chien, C.-C. Chiu, Y.-T. Cheng, W.-L. Fang, and E. H. Lim, "Multi-objective function for SWIPT system by SADDE," *Appl. Sci.*, vol. 10, no. 9, p. 3124, 2020.

[53] K. Xu, M. Zhang, J. Liu, N. Sha, W. Xie, and L. Chen, "SWIPT in mMIMO system with non-linear energy-harvesting terminals: Protocol design and performance optimization," *EURASIP J. Wireless Commun. Netw.*, vol. 2019, no. 1, pp. 1–15, 2019.

[54] L. Li, R. Cai, H. Jiang, and X. Su, "Rate-energy tradeoff for SWIPT systems with multi-user interference channels under non-linear energy harvesting model," in *Proc. IEEE 89th Veh. Technol. Conf. (VTC-Spring)*, May 2019, pp. 1–6.

[55] X. Peng and J. Li, "Harvested energy maximization of SWIPT system with popularity cache scheme in dense small cell networks," *Wireless Commun. Mobile Comput.*, vol. 2019, pp. 1–14, Jul. 2019.

[56] R. Morsi, V. Jamali, D. W. K. Ng, and R. Schober, "On the capacity of SWIPT systems with a nonlinear energy harvesting circuit," in *Proc. IEEE Int. Conf. Commun. (ICC)*, May 2018, pp. 1–7.

[57] Y. Lu, K. Xiong, P. Fan, Z. Ding, Z. Zhong, and K. Letaief, "Global energy efficiency in secure MISO SWIPT systems with non-linear power-splitting EH model," *IEEE J. Sel. Areas Commun.*, vol. 37, no. 1, pp. 216–232, Jan. 2019.

AJIN R. NAIR (Graduate Student Member, IEEE) received the B.Tech. degree in electronics and communication engineering from Amrita Vishwa Vidyapeetham, Bengaluru, and the M.Tech. degree in VLSI design from Amrita Vishwa Vidyapeetham, Coimbatore.

He is a Research Scholar at the Department of Electronics and Communication Engineering, Amrita School of Engineering, Coimbatore Campus. Before joining as a Research Scholar, he worked as an Application Developer in telecommunication at IBM India Pvt. Ltd., Bengaluru, for two years and has teaching experience of about five years in electronics communication engineering. He is currently working on the hardware impairment aspects in SWIPT-enabled wireless energy harvesting networks. He is an Associate Member of the Institution of Electronics and Telecommunication Engineers and a Lifetime Member of the Indian Society for Technical Education.

S. KIRTHIGA received the B.E. degree in electronics and communication from the Coimbatore Institute of Technology, in 1996, the M.E. degree in communication systems from the PSG College of Technology, in 2003, and the Ph.D. degree in millimeter wave communication from Amrita Vishwa Vidyapeetham, in 2015.

She worked as a Research and Development Engineer at Tata Elxsi, Bengaluru, from 1996 to 1999. In 2003, she joined the Amrita School of Engineering, Coimbatore, where she is currently an Associate Professor at the Department of Electronics and Communication Engineering. She has been actively involved in teaching and research activities with quality publications. She has been a Principal Investigator for the project funded by the Space Application Centre, ISRO. Her research interests include energy harvesting and SWIPT systems, land mobile satellite systems, wireless sensor networks, resource allocation using NOMA, and computational optimization using mobile edge computing. She is a member of the Institution of Electronics and Telecommunication Engineers. She has served as a reviewer for national and international conferences and journals.

• • •